Economic Geology, v. 102, pp. 667–690

Fracture Analysis of a Volcanogenic Massive Sulfide-Related Hydrothermal Cracking Zone, Upper Bell River Complex, Matagami, Quebec: Application of Permeability Tensor Theory

S. E. Ioannou[†,*] and E. T. C. Spooner

Department of Geology, University of Toronto, 22 Russell Street, Toronto, Ontario, Canada M5S 3B1

Abstract

Located in the Matagami mining district of the Abitibi greenstone belt, Quebec, the Bell River Complex is a >5-km-thick tholeiitic layered gabbro and/or anorthosite body (2724.6 +2.5/-1.9 $Ma_{U\text{-}Pb}$), which likely acted as the heat source that drove hydrothermal convection and volcanogenic massive sulfide (VMS) hydrothermal mineralization in the area.

Abundant fractures and veins crosscutting the western lobe of the Bell River Complex formed over a range of temperatures from 250° to 700°C. The 250° to 400°C assemblage, quartz-epidote ± sericite ± chlorite ± plagioclase, is the most widespread and occurs as orthogonal, anastomosing, and random vein sets. Vein densities average between 15 and 25 veins per m^2, locally reaching as high as 40 to 60 veins per m^2. These veins, typically 1 to 3 mm wide, are interpreted to represent thermal cracking associated with hydrothermal fluid mineralization in the district. Furthermore, they crosscut earlier higher temperature pyroxene-plagioclase (>600°C) and magnetite-rich (300°–600°C) veins (1–10 mm wide; densities commonly ~0–5 veins per m^2).

Detailed field measurements of quartz-epidote vein geometries coupled with permeability tensor theory have produced a first-order approximation of the maximum model permeability structure (veins unfilled) of the hydrothermal cracking zone. Representative district-wide values indicate maximum model bulk permeabilities of 10^{-10} to 10^{-8} m^2 for the hydrothermal cracking zone; similar to permeabilities calculated for the fractured sheeted dike complexes of the Semail and Troodos Ophiolites. However, a high-flow zone located within the central parts of the hydrothermal cracking zone is characterized by a maximum model permeability of 10^{-7} m^2. Locally (<1 m^2), the high-flow zone reaches maximum model permeability values as high as 10^{-6} to 10^{-5} m^2 where two or more veins occur with apertures in excess of 2 cm.

Mapping has shown that the hydrothermal cracking zone is confined to an ~350-m-thick interval located within a strongly layered gabbro and/or anorthosite horizon of the Layered zone, upper Bell River Complex. The base of this interval is 1,000 m below the top of the Bell River Complex. Furthermore, in and around the town of Matagami, the dominant orientation of quartz-epidote veins parallels the orientation of the layering (110° ± 15°). This parallelism is further reflected in the orientation of the calculated quartz-epidote vein permeability tensors (94° ± 30°, 1σ, n = 71). The parallelism suggests that heterogeneities associated with the layer contacts provided planes of low tensile strength along which the hydrothermal cracks preferentially developed. Such an interpretation further explains why the hydrothermal cracking zone appears to be restricted to the strongly layered zone; there are many more low tensile strength planes.

Zones of quartz-epidote veining approximately orthogonal to layering are also present. The orthogonal veins are usually less continuous and commonly truncated (but not crosscut) by layer-parallel veins. The orthogonal subset of veins is interpreted to represent short pathways that allowed fluids to travel between adjacent layer-parallel veins. However, locally, longer layering-orthogonal quartz-epidote veins, showing offsets of 10 to 30 cm normal to the layering of the Bell River Complex, may represent initial conduits that allowed fluids to travel into overlying stratigraphy and through to the paleosea floor.

Although volumetrically small in comparison with the permeability structure of the bulk sea floor, the significantly higher permeability of the hydrothermal cracking zone indicates its importance in controlling the flow paths and fluxes of fluids deep within the hydrothermal system.

Introduction

It has long been recognized that subvolcanic intrusions play a key role in the formation of volcanogenic massive sulfide (VMS) deposits. Not only do such intrusions provide the heat source necessary to drive large-scale hydrothermal convection, but it has also been suggested that they may contribute directly to the metal budget of the system (e.g., de Ronde, 1995; Alt, 1995; Yang and Scott, 1996; Schardt et al., 2005; Ioannou et al., 2007). Moreover, a temperature dependence on permeability has been recognized in the direct vicinity of magma chambers that can be envisioned as a hydrothermal cracking front or zone into which fluids are focused.

First described by Lister (1972, 1974, 1975, 1982, 1983, 1986) and later analyzed and modeled in more detail by Cathles (1983, 1993), the hydrothermal cracking zone forms in rocks that are cooled during thermal contraction along the margin of a thermal boundary layer adjacent to (within ~180 m for a dike model) the hot parts (>1,200°C) of an intrusion. The hydrothermal cracking zone acts as a primary zone of enhanced permeability which allows significant volumes of convecting fluid to flow around the intrusion, acquiring heat (>350°C) and dissolved components, including metals (e.g., Norton and Knight, 1977; Ioannou et al., 2007), before subsequently discharging through sea-floor black smoker vents.

[†] Corresponding author: e-mail, sioannou@haywood.com

[*] Current Address: Haywood Securities Inc., 181 Bay Street, Suite 2910, Toronto, Ontario, Canada M5J 2T3.

Furthermore, the cracking zone provides a site for the generation of saline brines through hydrothermal fluid phase separation; brines that are important for the dissolution and transport of metals in solution (Cathles, 1993; Ioannou et al., 2007).

Debate exists regarding the temperature over which hydrothermal cracking develops. For example, Fournier (1987, 1988) suggested that cracking fronts may develop in quasi-plastic crystalline rocks at temperatures as high as 750° to 800°C. However, calculations and computer simulations by Cathles (1983, 1993) and Barrie et al. (1999) indicate that most hydrothermal cracking occurs at temperatures between 275° and 375°C. At temperatures greater than 375°C, permeability within the hydrothermal cracking zone decreases from rapid dissolution of fracture contact points at the irregularities along fracture walls, with subsequent fracture closure at higher temperatures, thereby preventing the hydrothermal cracking from penetrating the thermal boundary layer of the intrusion except on a transient basis (Brantley et al., 1990; Cathles, 1993; Wilcock and Delaney, 1996; Zhang et al., 2001). Conversely, heat balance and thermal buoyancy attract the hydrothermal cracking front to the margin of the thermal boundary layer (Cathles, 1993).

Hydrothermal cracking is a well-documented phenomenon (e.g., Grímsvötn geothermal system, Iceland: Björnsson et al., 1982). Field observations support thermal cracking in and around well-preserved intermediate and mafic intrusions (e.g., Manning and Bird, 1986; Schiffries and Skinner, 1987), in ophiolite settings (e.g., Nehlig and Juteau, 1988; Nehlig, 1994; van Everdingen, 1995; Gillis and Roberts, 1999), and in deep exposures of in situ oceanic crust (e.g., Gillis, 1995; Manning et al., 1996). However, despite documentation of thermal cracking in numerous geologic environments, little has been done to quantify the physical properties associated with this process. Accurate modeling of VMS and other ore-forming systems requires a thorough understanding of key physical input parameters, including representative permeability values (e.g., Carr, 2004). Without realistic inputs, supported by field data, the validity of any given model is questionable. The following study investigates permeability limits that can be expected in a hydrothermal cracking zone. The values obtained are based on permeability tensor calculations made from field measurements collected in the Matagami VMS district of Quebec, which preserves clear evidence of hydrothermal cracking within its exposed subvolcanic intrusion, the Bell River Complex.

Geologic Setting

Located in the Harricana-Turgeon belt of the northern Abitibi subprovince, Quebec (Lacroix et al., 1990), the Matagami mining camp is one of the largest multideposit VMS districts in the Abitibi greenstone belt, containing in excess of 40 million metric tons (Mt) of massive sulfide ore, second only to Rouyn-Noranda (~103 Mt excluding the Horne 5 zone; Kerr and Gibson, 1993). Detailed descriptions of the geology of the Matagami district can be found in Sharpe (1965, 1968), Roberts (1975), Beaudry and Gaucher (1986), and Piché et al. (1993). In brief, the stratigraphy of the district consists of a lower, dominantly felsic volcanic package known as the Watson Lake Group (>1 km thick; 2724.5 ± 1.8 $Ma_{U\text{-}Pb}$: Mortensen, 1993), which is overlain by a dominantly mafic volcanic package known as the Wabassee Group (>13 km thick). A thin (2–4 m thick) unit of pyritic laminated cherty tuff known as the Key Tuffite marks the division between the two groups (Davidson, 1977; Liaghat and MacLean, 1992). The unit is a chemical exhalative sedimentary rock averaging 1.4 wt percent Zn and 0.1 wt percent Cu (Davidson, 1977), which has been interpreted to be genetically related to the VMS deposits that also occur, for the most part, at the contact between the Watson Lake and Wabassee Groups.

The Bell River Complex, originally described by Freeman (1939), is a >5-km-thick, layered tholeiitic gabbro and/or anorthosite body (2724.6 +2.5/-1.9 $Ma_{U\text{-}Pb}$: Mortensen, 1993) that intrudes the lower Watson Lake Group. Many, including Piché et al. (1990) and Maier et al. (1996), have suggested that the Bell River Complex acted as the heat source responsible for driving Archean VMS-related hydrothermal circulation in the area. Supporting evidence includes the fact that Bell River Complex granophyre, found in the uppermost level of the intrusion, and the Watson Lake Group rhyolite are compositionally identical and have ages that overlap within low uncertainties (+2.5/-1.9 $Ma_{U\text{-}Pb}$: Mortensen 1993). In addition, geochemical similarities to the Watson Lake and Wabassee Group tholeiitic basalts suggest that these lithologic units were derived through fractionation processes associated with the Bell River Complex (Scott, 1980; MacGeehan and MacLean, 1980a, b). A relatively continuous Mg-Fe fractionation trend across the Bell River Complex suggests that it was formed primarily through one large continuous intrusive event (Maier et al., 1996). However, gabbro sills cut the VMS deposits, Watson Lake Group rocks, and Wabassee Group rocks, indicating that less voluminous Bell River Complex-like magmas (based on field relationships and similar REE patterns) were emplaced after VMS formation and (early) deposition of the Wabassee Group (Scott, 1980; Maier et al., 1996). Multiphase intrusions spatially associated with VMS systems, which include pre- and/or syn- and post-VMS phases, are not uncommon (e.g., Galley et al., 2000a, b). At Matagami, available data suggest that a bulk of the Bell River Complex was emplaced prior to and/or during VMS formation.

Abundant fractures and veins crosscutting the western lobe of the Bell River Complex formed over a range of temperatures from 250° to 700°C. The 250° to 400°C assemblage, quartz-epidote ± sericite ± chlorite ± plagioclase (cf. Kristmannsdóttir, 1979; Richardson et al., 1987; Schiffman and Smith, 1988; Harper, 1999), is the most widespread and occurs as parallel, orthogonal, anastomosing, and random vein sets (Fig. 1). Vein densities average between 15 and 25 veins per m^2, locally reaching as high as 40 to 60 veins per m^2. These veins range from 1 to 60 mm wide, averaging 1 to 3 mm, and are interpreted to represent thermal cracking associated with hydrothermal fluid flow during VMS deposit formation in the district. The fineness of these veins is consistent with hydrothermal cracking zone-type veins found in plutonic rocks in ophiolite settings (Nehlig, 1991, 1993). Furthermore, these veins crosscut and offset, up to 50 cm locally, high-temperature, pyroxene-plagioclase (>600°C, e.g., Schiffries and Skinner, 1987) and magnetite-rich (300°–600°C, e.g., Schiffries and Skinner, 1987) veins ranging from 1 to 45 mm

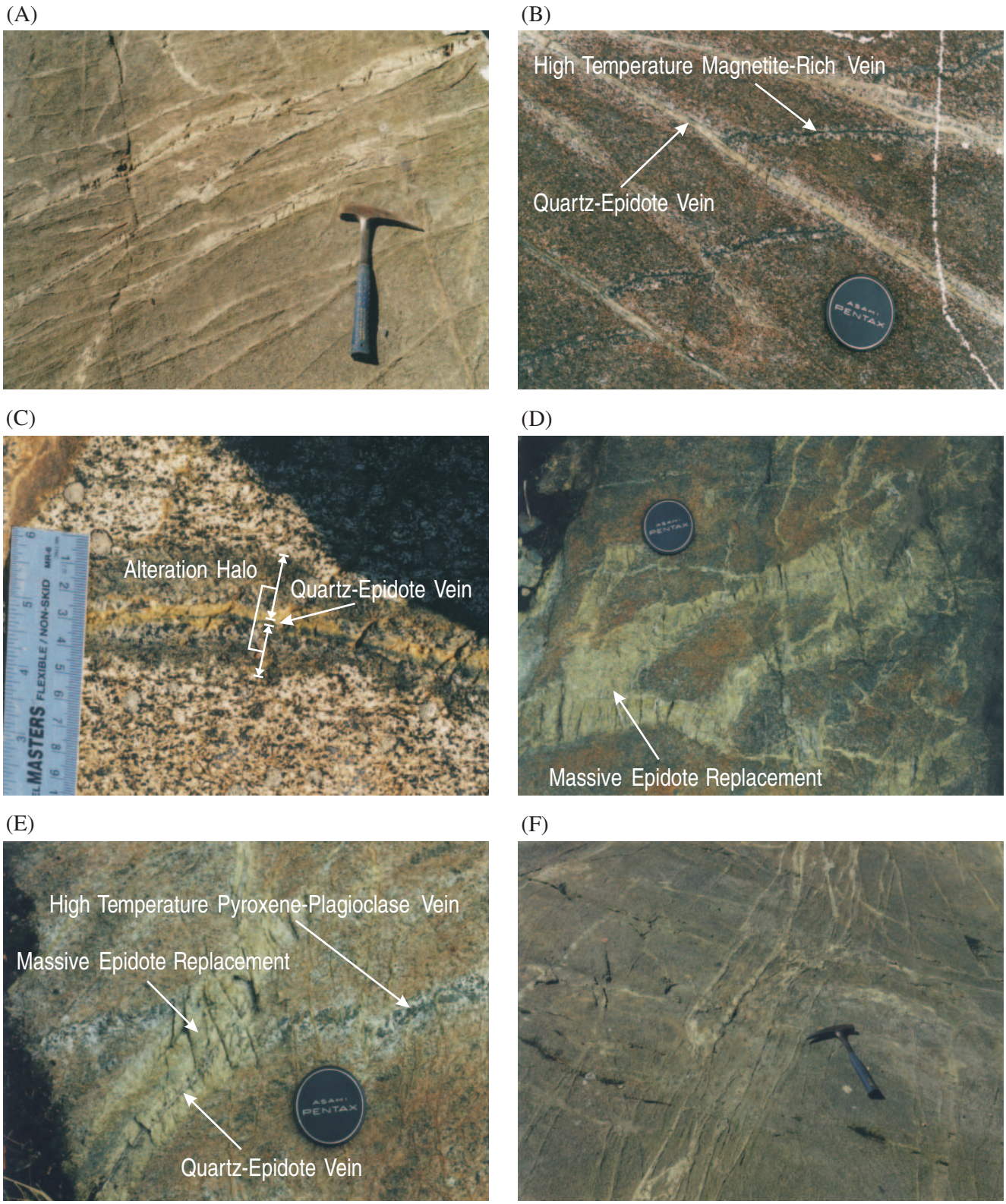

FIG. 1. A-F. Quartz-epidote veining associated with the hydrothermal cracking zone of the Bell River Complex in and around the town of Matagami. Note the quartz-epidote veins crosscutting and offsetting earlier high-temperature magnetite-rich veins in (B). A typical quartz-epidote vein alteration halo is shown in (C). Massive epidote replacement of host gabbro is shown in (D).

wide (Fig. 1B). Densities of ~0 to 5 veins per m^2 are common for these higher temperature veins but locally reach more than 30 veins per m^2 , in part reflective of possible supersolidus conditions (e.g., Manning and Bird, 1986; Nehlig and Juteau, 1988; Nicolas et al., 1988).

Alteration halos, 5 to 30 mm in thickness, commonly flank the quartz-epidote veins (Fig. 1C). The contact between vein and altered host rock is usually clear and sharp, as is the transition from altered to unaltered host rock. However, locally, epidote alteration is more extensive, forming irregular vein-like masses that clearly replace the host gabbro and/or anorthosite (Fig. 1D) and are similar in appearance to epidosite mineralization observed in other VMS systems (e.g., Richardson et al., 1987; Schiffman and Smith, 1988; Nehlig et al., 1994; Harper, 1999). This massive epidote alteration was avoided during vein measurement and subsequent permeability analysis. Conversely, the high-temperature pyroxene-plagioclase veins have no alteration halos and the magnetite-rich veins are characterized by narrow white alteration halos typically measuring about one-third of the vein's width, similar to the high-temperature veins described by Schiffries and Skinner (1987). The thin to nonexistent halos in these veins are likely a result of rapid healing under high-temperature conditions, in effect limiting the development of diffusion-controlled alteration (Cathles, 1993).

Regional deformation synchronous with and postdating the intrusion of the Bell River Complex and VMS mineralization formed the westward-plunging district-scale Galinée anticline (Piché et al., 1993). Subsequent erosion has exposed the Bell River Complex along the axis of the anticline and two volcanic belts on the north and south limbs (Fig. 2). Younger banded-iron formation and clastic sedimentary rocks, primarily siltstones, argillites, and minor granitoid pebble conglomerates of the Matagami and Taibi Groups, conformably bound these limbs to the north and south, respectively (Beaudry and Gaucher, 1986).

Postvolcanic to post-tectonic intrusions of varying compositions (dioritic, tonalitic, granodioritic) occur throughout the district and include the Olga, Desmazures, Cavelier, and Dunlop Bay plutons. In addition, Proterozoic diabase dikes intrude the stratigraphy throughout the western part of the camp (Piché et al., 1993).

Twenty VMS deposits with tonnages ranging from ~0.1 to more than 25 Mt have been discovered in the Matagami

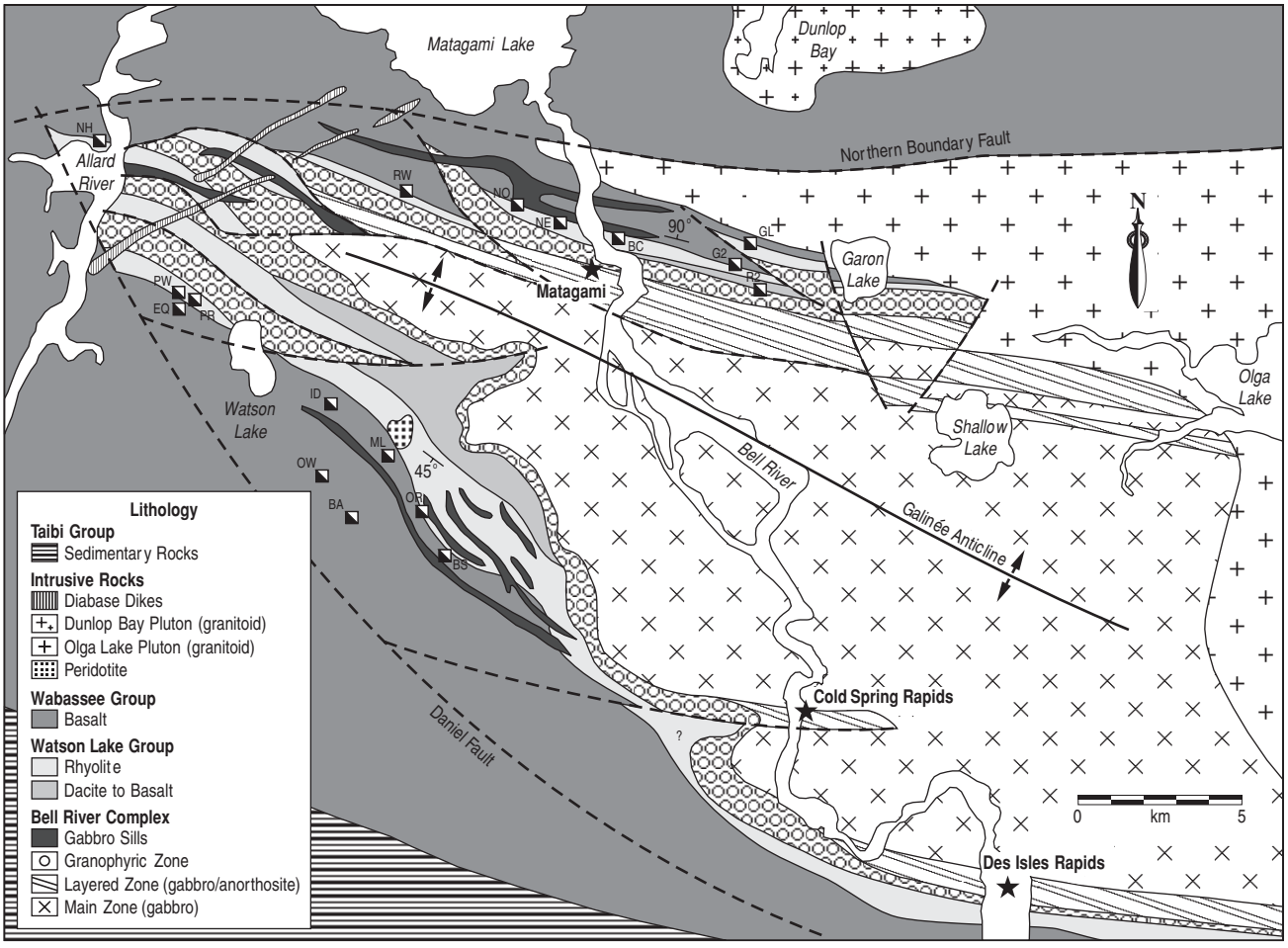

FIG. 2. Geologic map of the Matagami district (modified from Piché et al., 1993; Maier et al., 1996). North-limb deposits: BC = Bell Channel, GL = Garon Lake, G2 = Garon Lake 2, NE = Norita East, NH = New Hosco, NO = Norita, RS = Radiore 2, RW = Radiore West. South-limb deposits: BA = Bell Allard, BS = Bell Allard South, EQ = Equinox, ID = Isle-Dieu, ML = Mattagami Lake, OR = Orchan, OW = Orchan West, PR = Perseverance, PW = Perseverance West.

district since 1956. The deposits are typically Zn rich, averaging ~9 and reaching as high as 17.6 wt percent Zn (e.g., Isle-Dieu). Cu grades are significantly lower, averaging ~1 and do not exceed 2 wt percent Cu.

Field Methodology

A 1-m^2 (square) frame was used to measure veins systematically in a manner similar to the study of Haynes and Titley (1980). At each measurement site, the frame was placed so that one of its diagonals corresponded to a north-south orientation (Fig. 3A). Veins lying within the frame were counted and measured for strike direction, length within the frame, aperture (taken as an approximation of the vein's average aperture) and, where available, dip. The veins were further classified as either high temperature (i.e., pyroxene-plagioclase or magnetite-rich) or quartz-epidote. Veins that were clearly not associated with either of these mineralogical classifications (i.e., not interpreted as related to VMS mineralization), rare in the study area, were omitted. In total 1,436 veins were measured (Table 1, Fig. 4). Although every effort was made to obtain data in three dimensions, many of the good outcrops in the study area are relatively flat, typical of glaciated terranes, making dip measurements difficult or impossible. Measured sites were selected based on the quality of vein exposure; locally, moss and lichen cover are very thick, making it difficult to measure veining accurately. Furthermore, sites most representative of an entire outcrop or area were given priority. In addition to measured sites, numerous localities of rocks that were barren of cracks (i.e., zero fracture permeability) were also noted during mapping and for subsequent interpretations of the hydrothermal cracking zone.

Permeability Calculation

In situ field tests (e.g., hydraulic conductivity; Wilson et al., 1983) are commonly used to estimate the permeability of porous media but cannot be applied to ancient rocks in which paleofluid pathways are filled with mineral precipitates or affected by geologically late hydrologic modifications (e.g., fracturing; jointing) not associated with the system in question. An alternate approach, such as numerical modelling, is needed to model the paleohydrology of ancient systems.

Simple theoretical cubic relationships between fracture geometry and the resultant permeability, based on parallel-plate concepts such as $k = nd^3/12$ (derived from laboratory and in situ experiments where k is permeability, n is fracture

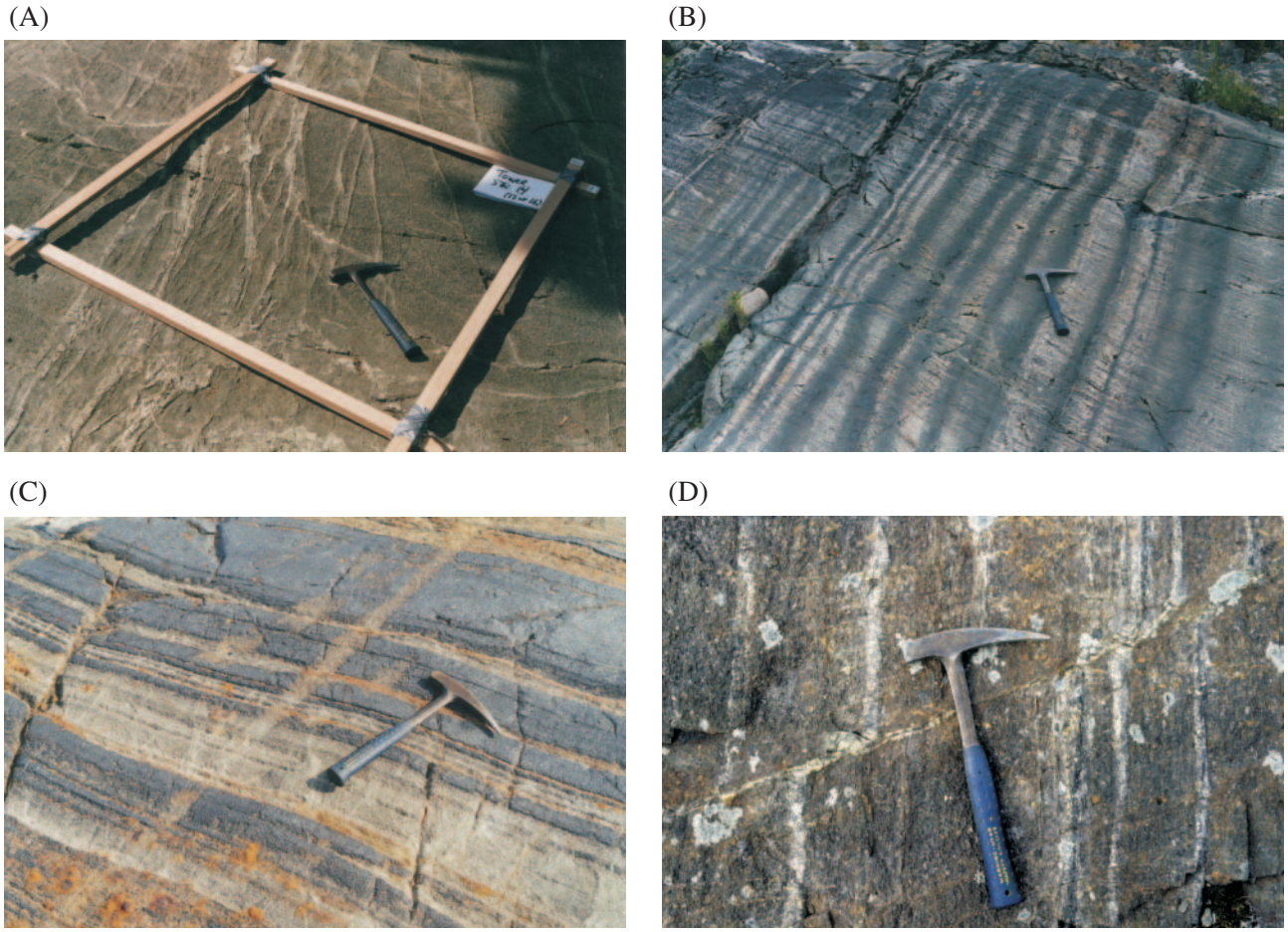

FIG. 3. Field photographs of layering and veins in the Bell River Complex. A. 1-m^2 fracture measurement frame. B. Strongly layered zone, Upper Bell River Complex, Cold Spring Rapids area. C. Layered magnetite-rich horizon, Upper Bell River Complex, north of Shallow Lake (see Fig. 2). D. Layering-orthogonal quartz-epidote vein, town of Matagami. Note the normal offset of Bell River Complex layering across the vein.

TABLE 1. Summary of Two- and Three-Dimensional Fracture Data and Tensor Results (k_1, k_2) for Quartz-Epidote and High-Temperature Veins

Two-dimensional fracture data

Area	Quartz-epidote veins Aperture (mm)	Quartz-epidote veins Strike (°)	High-temperature veins Aperture (mm)	High-temperature veins Strike (°)
Matagami	(1.0 to 60.0) n = 1088	(000 to 175) n = 1088	(1.0 to 45.0) n = 39	(050 to 125) n = 39
Cold Spring	1.7 ± 4.6 (1.0 to 60.0) n = 171	025 ± 45 (000 to 179) n = 171	1.3 ± 0.3 (1.0 to 1.5) n = 33	161 ± 031 (010 to 140) n = 171
Des Isles	1.5 ± 0.7 (1.0 to 4.0) n = 66	165 ± 42 (010 to 179) n = 66	2.0 ± 1.6 (1.0 to 11.0) n = 39	007 ± 045 (020 to 173) n = 39

Two-dimensional permeability results for quartz-epidote veins

Area	Log(k_1) (m²)	k_1 trend (°)	Log(k_2) (m²)	k_2 trend (°)
Matagami (n = 71)	–10.1 ± 2.4 (–18.0 to –8.0)	004 ± 30 (000 to 178)	–7.5 ± 1.3 (–10.0 to –5.0)	094 ± 30 (028 to 150)
Cold Spring (n = 5)	–9.2 ± 0.8 (–10.0 to –8.0)	106 ± 31 (080 to 152)	–8.4 ± 2.1 (–10.0 to –5.0)	016 ± 31 (001 to 174)
Des Isles (n = 4)	–9.8 ± 0.5 (–10.0 to –9.0)	101 ± 20 (087 to 130)	–9.0 ± 0.0 (–9.0 to –9.0)	011 ± 20 (009 to 180)

Two-dimensional permeability results for high-temperature veins

Area	Log(k_1) (m²)	k_1 trend (°)	Log(k_2) (m²)	k_2 trend (°)
Matagami (n = 20)	–15.0 ± 3.5 (–18.0 to –9.0)	169 ± 26 (000 to 175)	–9.3 ± 1.0 (–11.0 to –7.0)	079 ± 26 (050 to 125)
Cold Spring (n = 1)	–10.0	051	–9.0	141
Des Isles (n = 3)	–12.7 ± 4.6 (–18.0 to –10.0)	110 ± 14 (095 to 121)	–8.7 ± 0.6 (–9.0 to –8.0)	020 ± 14 (005 to 031)

Notes: Top number expresses the mean (± corresponds to 1σ); bracketed numbers express the range; n = the number of measurements

Three-dimensional fracture data

Vein type	Aperture (mm)	Strike (°)	Dip (°)
Quartz-Epidote (n = 38)	4.7 ± 7.7 (1.0 to 45.0)	094 ± 26 (045 to 120)	–83S ± 17 (–30S to –75N)
High Temperature (n = 2)	8.0 ± 5.7 (4.0 to 12.0)	080 ± 0 (080 to 080)	–85S ± 4 (–82S to –88S)

Three-dimensional permeability tensor results for quartz-epidote veins

Component	Log(k) (m²)	Trend (°)	Plunge (°)
k_1 (n = 4)	–9.5 ± 1.3 (–11.0 to –8.0)	022 ± 4 (019 to 028)	5 ± 5 (0 to 11)
k_2 (n = 4)	–7.0 ± 0.8 (–8.0 to –6.0)	135 ± 42 (017 to 119)	–7 ± 55 (–79 to 36)
k_3 (n = 4)	–7.0 ± 0.8 (–8.0 to –6.0)	109 ± 6 (102 to 115)	–9 ± 60 (–56 to 73)

Three-dimensional permeability tensor results for high-temperature veins

Component	Log(k) (m²)	Trend (°)	Plunge (°)
k_1 (n = 1)	–11.0	035	10
k_2 (n = 1)	–7.0	125	0
k_3 (n = 1)	–7.0	033	–80

TABLE 1. *(Cont.)*

Comparison of two- vs. three-dimensional permeability tensors for quartz-epidote veins[1]

Component	Two-dimensional calculation (n = 4)	Three-dimensional calculation (n = 4)
Log(k_1) (m²)	–9.5 ± 1.3 (–11.0:–8.0)	–9.5 ± 1.3 (–11.0:–8.0)
Log(k_2) (m²)		–7.0 ± 0.8 (–8.0:–6.0)
Log(k_3) (m²)	–7.0 ± 0.8 (–8.0:–6.0)	–7.0 ± 0.8 (–8.0:–6.0)
k_1 trend (°)	022 ± 4 (019:028)	022 ± 4 (019:028)
k_2 trend (°)	112 ± 4 (109:118)	135 ± 42 (017:119)
k_3 trend (°)		109 ± 6 (102:115)

[1] Two-dimensional results are calculated from sites which yielded both two- and three-dimensional data

abundance, and d is fracture aperture), have been known for some time (e.g., Snow, 1965, 1968, 1970; Norton and Knapp, 1977; Brace, 1980). The validity of such cubic relationships has been demonstrated in the laboratory for superfine fractures with apertures down to 0.2 μm (Romm, 1966). In naturally occurring materials, such as marble and granite with characteristically rougher surfaces, cubic relationships have been shown to be valid for fracture apertures down to 10 μm (Witherspoon et al., 1980; Gale, 1982; Zimmerman and Yeo, 2000).

Vilas and Norton (1977), Haynes and Titley (1980), and Nehlig and Juteau (1988) have used such relationships to estimate first-order paleopermeabilities in and around the Mayflower stock, Utah, the Ruby Star Granodiorite, Arizona, and in sheeted dikes and gabbros in parts of the Oman ophiolite, respectively. However, full two- and three-dimensional permeability tensor theory, pioneered by Snow (1969) and Bianchi and Snow (1969), and advanced by Oda (1983, 1984, 1985, 1986) and Oda et al. (1987), has not been applied directly to ore-forming systems. In permeability tensor theory, the discharge from one planar fracture or any set of planar fractures can be represented by a second-rank tensor. The tensor describes the permeability of the continuous rock medium with the same discharge as a fractured medium under the same hydraulic gradient and laminar flow conditions. The main advantages of using tensor theory are that it accounts for the directional variability of individual fractures and ultimately provides a directionally specific permeability.

Tensor theory applied to field measurements is a proven method to model permeability accurately. For example, Oda et al. (1987) have compared numerically derived tensor data from fractures and/or joints with millimeter-scale apertures with field measurements obtained through large-scale hydraulic conductivity (Wilson et al., 1983) and packer injection tests (Gale and Rouleau, 1985) in granite from the Stripa mine, Sweden (Witherspoon, 2000). The comparisons demonstrate that the three different approaches yield the same (order of magnitude) results (10^{-17} m²).

Permeability tensor theory

A full derivation of the permeability tensor theory applied to this study is presented by Oda (1985) and is outlined in the Appendix. If a defined fractured rock mass volume can be considered a homogeneous anisotropic porous medium, it obeys Darcy's Law, which states that the apparent seepage velocity, v_i , is related to the gradient of total hydraulic head, ϕ, by a coefficient, k_{ij} , known as the permeability tensor (Oda, 1985)

$$v_i = -\frac{g}{\nu} k_{ij} \frac{\partial \phi}{\partial x_i} = \frac{g}{\nu} k_{ij} J_i, \quad (1)$$

where g is the gravitational acceleration, ν is the kinematic viscosity, and $J_i = -\partial\phi/\partial x_i$. As noted by Oda (1985), it is not guaranteed that every rock mass can be simulated by an equivalent porous medium with a symmetrical permeability tensor. However, numerical studies by Long et al. (1982) and Oda (1985) have indicated that rock masses containing a significant number of discontinuities do in fact approach such behavior.

Throughout this study it is assumed that the uncracked gabbro and/or anorthosite of the Bell River Complex are impermeable relative to the cracked rock, at least to a first-order approximation. As a result, fluid flow is restricted to the cracks. By considering a cubic flow region of volume V, homogeneously cut by $m^{(V)}$ cracks with diameter r and aperture t, Oda (1985) showed that equation (1) can be rewritten as:

$$v_i = \lambda \frac{g}{V} \left[\frac{\pi\rho}{4} \int_0^{t_{max}} \int_0^{r_{max}} \int_0^{\Omega} r^2 t^3 (\delta_{ij} - n_i n_j)\, E(\boldsymbol{n}, r, t)\, d\Omega\, dr\, dt \right] J_i, \quad (2)$$

where $\boldsymbol{n}$ is the unit vector normal to the plane of the cracks. Comparison of equation (2) with Darcy's Law (eq 1) yields an equivalent permeability tensor $k_{ij}^{(c)}$ for the crack system as follows (Oda, 1985):

$$k_{ij}^{(c)} = \lambda (P_{kk}\delta_{ij} - P_{ij}), \quad (3)$$

where

$$P_{ij} = \frac{\pi}{4V} \int_0^{t_{max}} \int_0^{r_{max}} \int_0^{\Omega} r^2 t^3 n_i n_j dN \quad (4)$$

and

$$P_{kk} = P_{11} + P_{22} + P_{33}, \quad (5)$$

where λ is a dimensionless constant and δ_{ij} is the Kronecker delta (see App.). P_{ij}, defined by Oda (1985) as the crack tensor, is a symmetric second-rank tensor related only to the crack geometry (length, aperture, orientation). Equation (3)

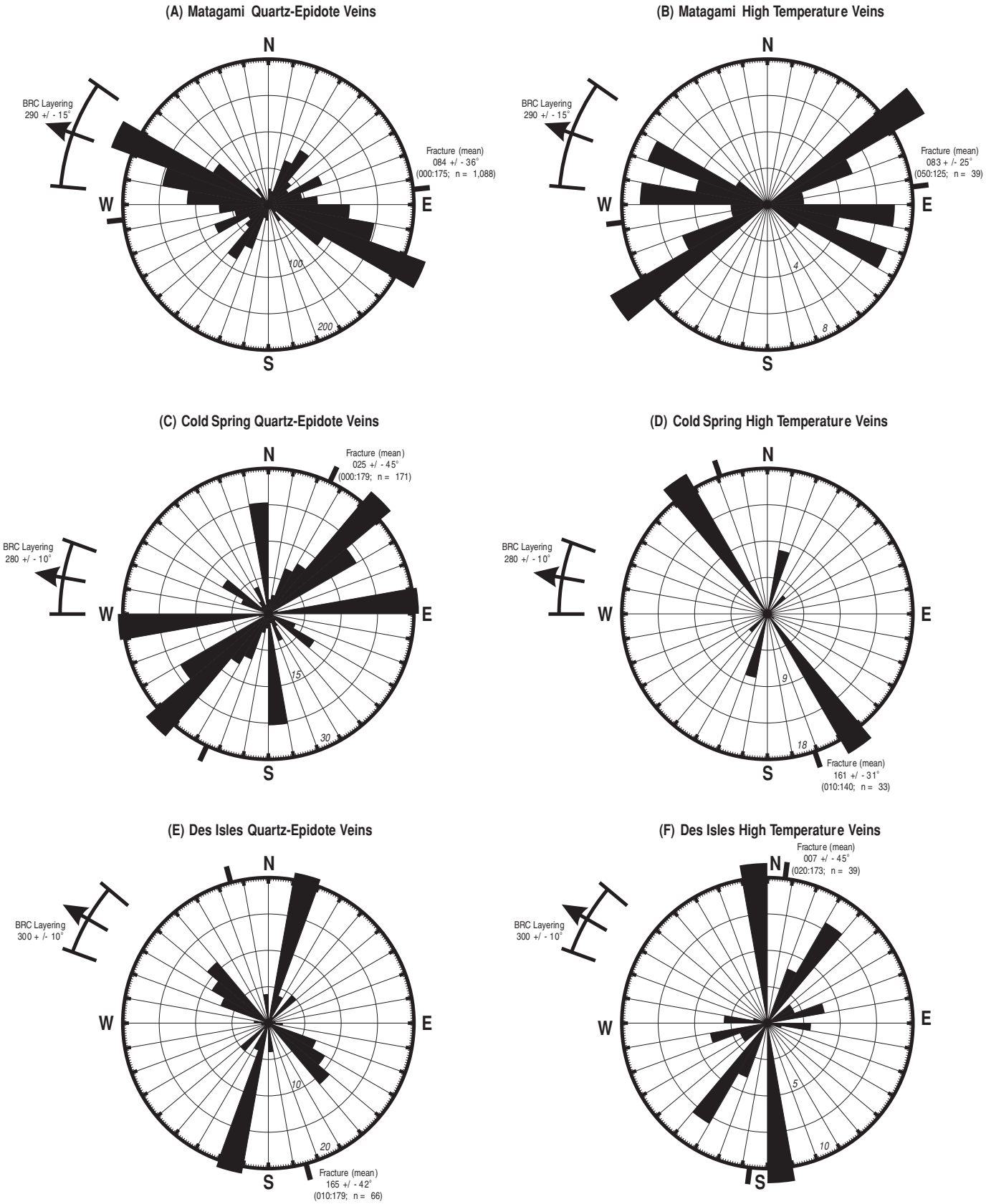

FIG. 4. Fracture orientation rose diagrams for Matagami (town), Cold Spring and Des Isles Rapids (fracture mean $\pm 1\sigma$; numbers in parentheses indicate the range; n = number of measurements).

assumes that the flow region is fully divided by cracks, thus providing multiple flow paths. Furthermore, equation (5) produces a nonzero permeability, even when P_{ij} becomes negligibly small. However, in actuality, the flow region (especially at larger scales) may become impermeable from a loss of connectivity between cracks. Oda (1985) provided a minor modification to equation (3) to account for such a scenario. However, it is omitted here because of the abundant cracks at all sample locations.

Application: As discussed above, a lack of outcrop exposure in the third dimension limited the collection of data and tensor calculations at a majority of the sample sites to two dimensions. However, three-dimensional data were obtained from five sites to complement two-dimensional data. The data from these five sites indicate that there are no significant discrepancies between the magnitude or orientation of the two- and three-dimensional permeability tensors calculated.

Results

Despite the rigorous nature of the permeability tensor calculation, the realities of making field measurements limit this type of study to order of magnitude estimates of permeability. For instance, moss and lichen, as well as weathering on numerous outcrops, likely masked a number of finer fractures, microscopic fractures, not visible in outcrop have been observed in thin section and likely contributed to the overall permeability of the rock volume, and, despite every effort to measure the distinct geometrical characteristics of each fracture, local generalizations were needed when the fractures became highly irregular and networked. Other unaccounted-for (not measurable) real physical parameters, such as continuity, tortuosity, and fracture roughness, also likely result in calculated permeability that differs from actual permeability. For example, Brown (1987) has shown that the surface roughness of fractures can retard flow by as much as 10 to 30 percent. Furthermore, highly localized (i.e., over areas <1 m^2) increases in fracture abundance and/or aperture can cause localized variations in permeability by as much as three orders of magnitude. Therefore, the order of magnitude estimates most realistically represent the permeability of the hydrothermal cracking zone over significant areas.

The permeability tensor calculation used in this study makes four assumptions:

1. Permeability is defined by the fractures; unfractured gabbro of the Bell River Complex is considered impermeable at ~10^{-24} m^2 (Trimmer et al., 1980; Fisher, 1998), although we acknowledge that the 2- to 30-mm-thick alteration halos characteristic of the quartz-epidote veins indicate some hydrothermal fluid penetration into the host rock
2. The fracture apertures measured reflect the original fracture aperture before infilling. The effects of mineral precipitation (or dissolution) and/or crack-seal cycling on permeability, difficult to accurately quantify, are not considered; permeability decreases cubically with decreasing aperture.
3. All fractures are interconnected and constitute the backbone network of the crack system (Cox et al., 2001).
4. All fractures of a given set (i.e., quartz-epidote or high-temperature veins) were open at the same time. This assumption is supported by a lack of crosscutting relationships in either fracture set and a general lack of secondary fluid inclusions in the quartz-epidote veins (Ioannou et al., 2007). Furthermore, the quartz-epidote veins produce a spatially homogeneous cathodoluminescence, indicative of a nonfluctuating hydrothermal fluid composition (Ioannou et al., 2004) and possibly a single hydrothermal event. Similar inferences based on field relationships have also been made at sites of hydrothermal cracking in ophiolite sequences (e.g., Nehlig, 1994).

Given these four assumptions, the model permeabilities calculated are interpreted as maximum values.

A total of 73 sites (1,127 veins) were measured in and around the town of Matagami (Table 1; Figs. 5–7). Figures 6 and 7 illustrate the distribution of vein (crack) density and permeability in the area and the calculated two-dimenaional permeability tensor orientation (Fig. 7). An additional 12 sites were measured in equivalent Bell River Complex stratigraphy at Cold Spring Rapids (6 sites, 204 veins) and Des Isles Rapids (6 sites, 105 veins) along the south limb of the Galinée anticline (Figs. 2, 4, 5; Table 1). The sites on the south-limb were measured to assess whether the hydrothermal cracking observed in and around the town of Matagami was typical or atypical of the fluid-flow system as a whole. The results obtained from the sites suggest that the hydrothermal cracking seen near the town of Matagami is representative of that which occurred throughout the district during the time of VMS mineralization. Localization of hydrothermal cracks to a particular stratigraphic horizon on both limbs of the Galinée anticline also supports a VMS-related hydrothermal origin (i.e., 2725 Ma; Mortensen, 1993) for the cracks.

The findings are consistent with work by Nehlig (1991, 1993) on the Semail ophiolite sequence, Oman, and by Dilles and Einaudi (1992) and Dilles et al. (1992) on the Yerington batholith, Nevada, which shows that surficial hydrothermal fluids are capable of penetrating the upper parts of crystallized magma chambers. At Matagami, this was likely aided by the shallow emplacement of the Bell River Complex to approximately 1,000 m below the paleosea floor (Roberts, 1975). Furthermore, Nehlig (1991, 1993) noted that fluid phase separation is limited to the pluton, as interpreted at Matagami (Ioannou et al., 2007). Separate permeability tensors were calculated for high-temperature veins and quartz-epidote veins, since crosscutting relationships very clearly show that these two vein types were active at different times (Fig. 1B, Table 1).

Representative district-wide values indicate a maximum bulk model permeability of 10^{-10} to 10^{-8} m^2 for the hydrothermal cracking zone at Matagami. However, a high-flow zone located within the central parts of the hydrothermal cracking zone is characterized by a maximum model permeability of 10^{-7} m^2. On a localized scale (<1 m^2), the high-flow zone reaches maximum model permeability values as high as 10^{-6} to 10^{-5} m^2 where two or more veins occur with apertures in excess of 2 cm.

The magnitudes of the district district-wide permeability calculated here (10^{-1}–10^{-8} m^2) are in good agreement with in situ measurements for fractured rocks (Brace, 1980) and field-based calculations for other VMS-related fracture systems (Nehlig and Juteau, 1988; van Everdingen, 1995; Table 2). Hence, they appear to be reasonable maximum model permeabilities.

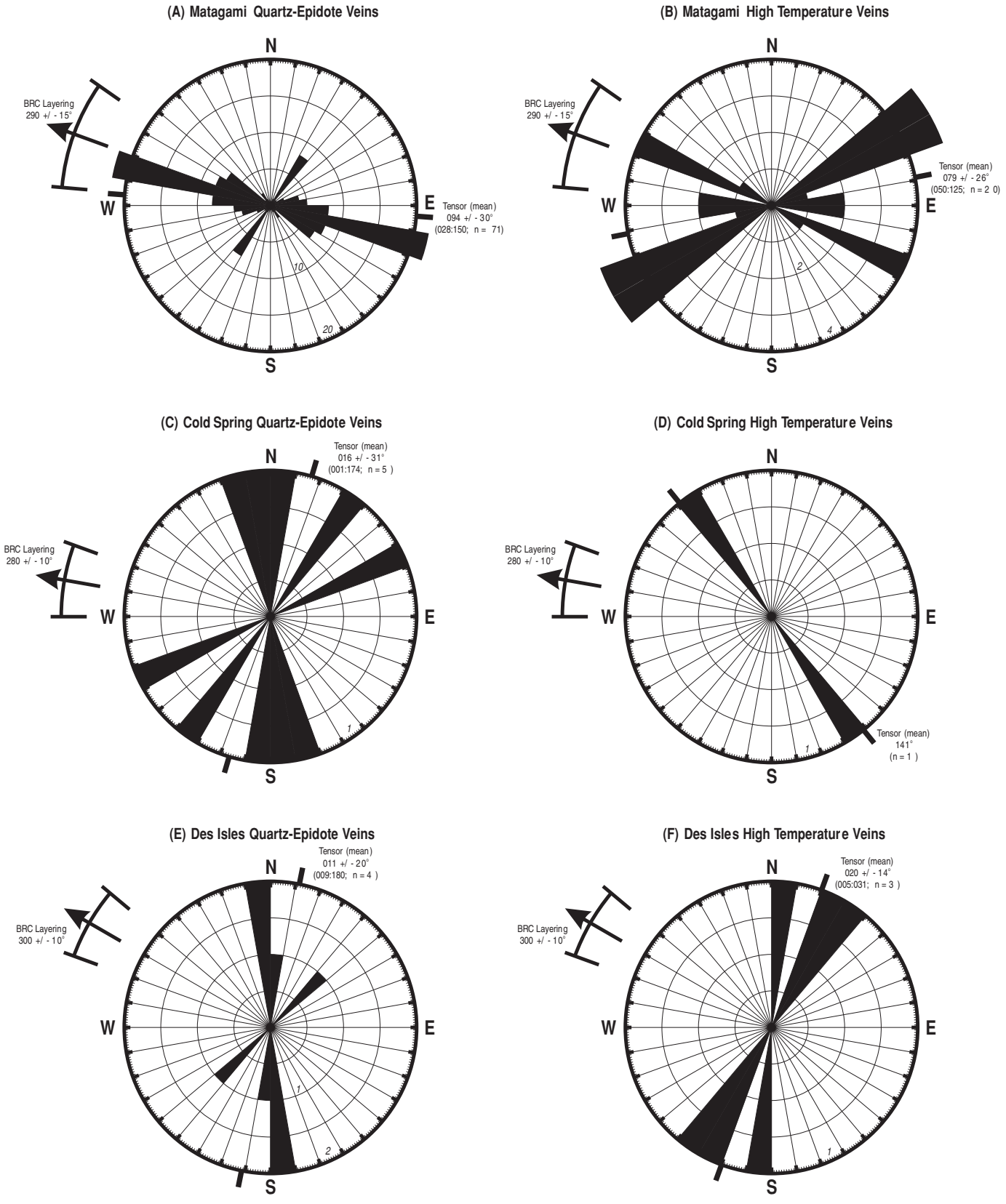

FIG. 5. Two-dimensional permeability tensor rose diagrams for Matagami (town), Cold Spring and Des Isles Rapids (tensor mean $\pm 1\sigma$; bracketed numbers indicate the range; n = number of measurements).

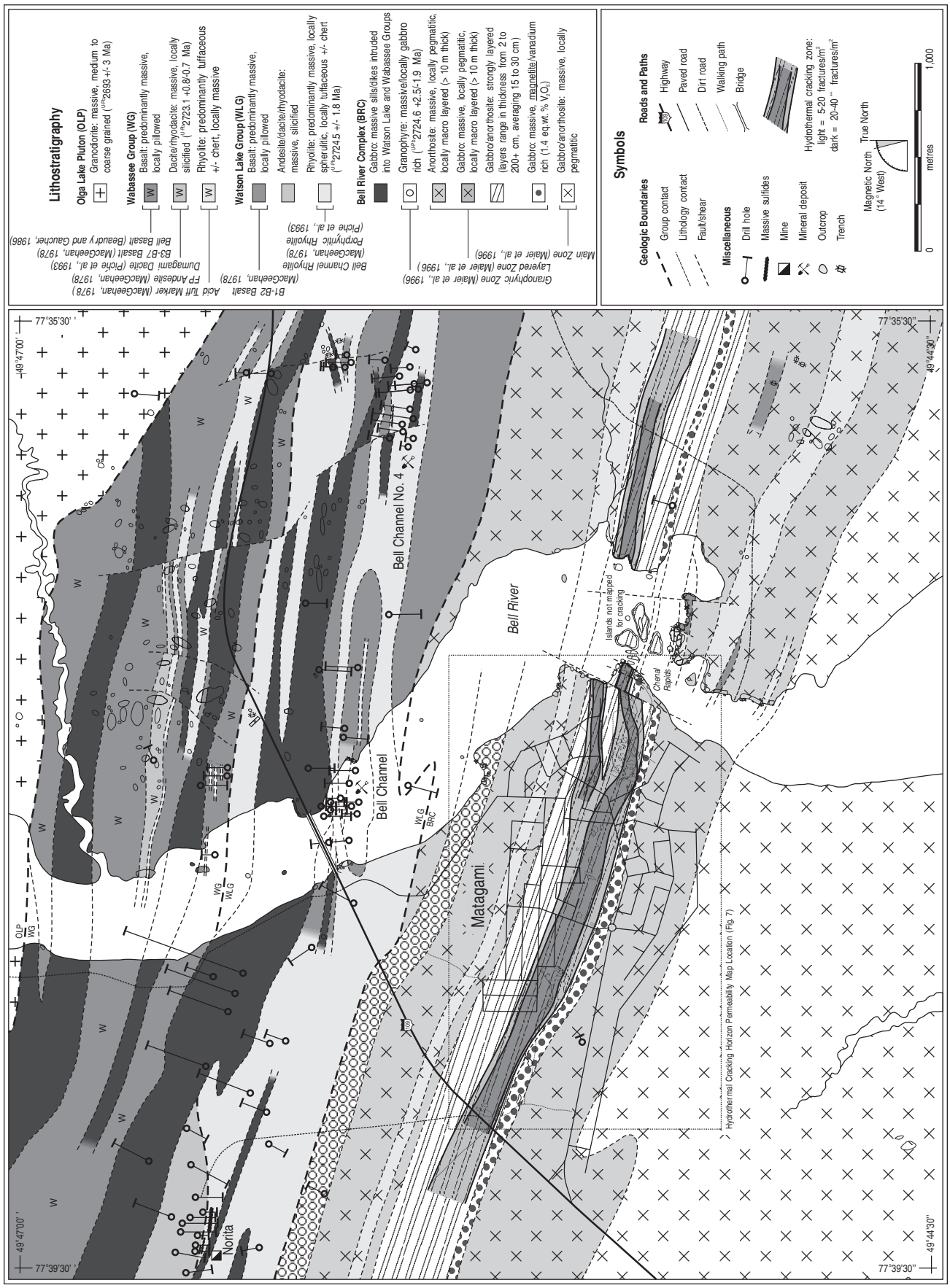

FIG. 6. North-limb geology in and around the town of Matagami, Quebec. Note that stratigraphy dips subvertically and youngs to the north. Mapping is based on field work carried out for this study and previous mapping (modified) by Sharpe (1968) and Beaudry and Gaucher (1986).

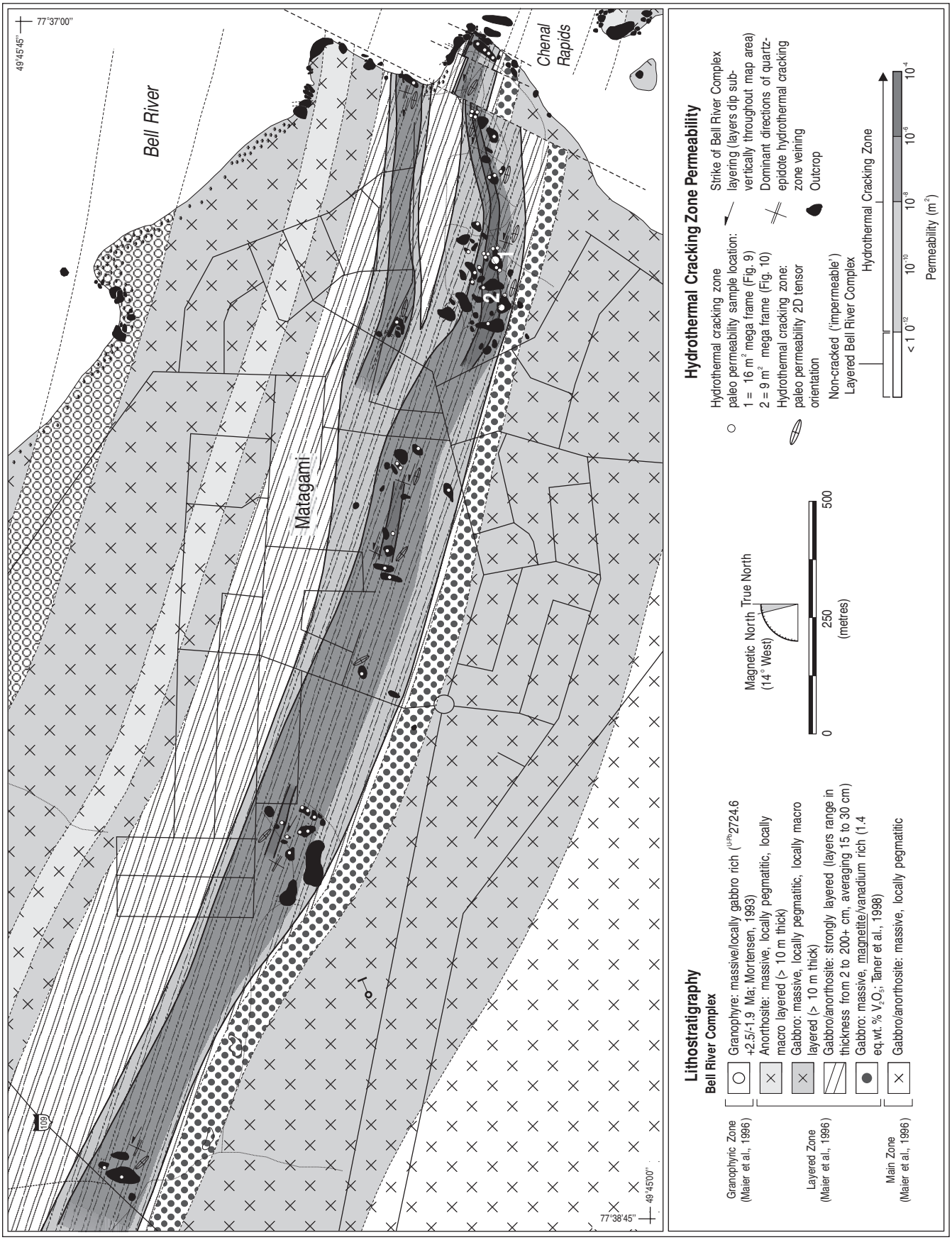

FIG. 7. Permeability map of the hydrothermal cracking zone of the Bell River Complex near the town of Matagami, Quebec.

TABLE 2. Comparison of Permeabilities Calculated for VMS and Porphyry-Related Systems

Location	k (m^2)	Method	Source
Semail Ophiolite, Oman (layer 2B - sheeted dike complex and upper plutonic sequence)	10^{-11} to 10^{-8}	Field measurement and basic permeability theory (Snow, 1970; Norton and Knapp, 1977)	Nehlig and Juteau (1988)
Troodos Ophiolite, Cyprus (layer 2B - sheeted dike complex)	10^{-12} to 10^{-6}	Field measurement and permeability tensor theory (Bianchi and Snow, 1969; Oda, 1985)	van Everdingen (1995)
Model VMS (basalts within 200 m of the sea floor; discrete 40-m-thick lateral zones of higher permeability)	10^{-9}	Heat and fluid flow theory (Bodvarsson, 1982)	Fisher and Becker (1995)
Model VMS (hydrothermal cracking front)	10^{-13} to $>10^{-10}$	Heat and fluid flow theory (Cathles, 1981)	Cathles (1993)
Matagami, Quebec (hydrothermal cracking horizon)	10^{-10} to 10^{-8}	Field measurement and permeability tensor theory (Bianchi and Snow, 1969; Oda, 1985)	This study
Mayflower Stock, Utah (porphyry system)	10^{-13} to 10^{-11}	Field measurement and basic permeability theory (Snow, 1970; Norton and Knapp, 1977)	Vilas and Norton (1977)
Ruby Star Granodiorite, Arizona (porphyry system)	10^{-15} to 10^{-12}	Field measurement and basic permeability theory (Snow, 1970; Norton and Knapp, 1977)	Haynes and Titley (1980)

Discussion

Geologic relationships between hydrothermal cracking and layering of the Bell River Complex

Detailed mapping of the upper Bell River Complex (Fig. 6) shows that the layered stratigraphy originally recorded by Sharpe (1968), Beaudry and Gaucher (1986), and Maier et al. (1996) can be further subdivided. Aside from a granophyric cap (<300 m thick), the upper 1.5 km of the Bell River Complex is dominated by an assemblage of layered gabbro and anorthosite. The magmatic layering is caused by variations in mineralogy and/or changes in grain size and texture. As noted by Scott (1980), both symmetrical layering and grading of minerals occurs (Wager and Brown, 1968), although the latter does not yield consistent top directions. Throughout the town of Matagami, and the north limb in general, the layering now dips subvertically as a result of folding and the development of the Galinée anticline.

Although predominantly macrolayered, with individual layers >>10 m thick, there is one distinct ~500-m-thick interval within the upper Bell River Complex, with a base ~1,000 m below the top of the intrusion, that shows more regularly spaced layering (the strongly layered zone; Fig. 3B). In some places, individual layers are only 5 to 10 cm thick. It is within this interval that hydrothermal cracking appears to be concentrated. This finding suggests that the hydrothermal cracking "front" terminology used by previous authors is not completely applicable in this case; hydrothermal cracking at Matagami is restricted to a discrete zone, measuring approximately 350 m in thickness, within the intrusion rather than to a front that sweeps across the intrusion from the outside in.

During mapping it was noted that the hydrothermal cracking zone stands in high relief, forming a ridge >10 m in height that extends across the town of Matagami. We interpret the ridge to be an indication of erosion-resistant material; likely a product of alteration, silicification, and quartz-epidote vein formation associated with hydrothermal cracking. In outcrop-barren areas within the strongly layered zone, a lack of topographic relief has been used to infer a lower density of hydrothermal cracking (Fig. 7). In fact, wherever the Bell River traverses hydrothermally cracked, strongly layered rocks, there are significant rapids (e.g., Chenel, Cold Spring, Des Isles; Figs. 2, 6) consistent with the hydrothermal cracking zone being characterized by erosion resistant material.

A distinct mappable vanadium-bearing magnetite horizon (±50 m thick) occurs stratigraphically at and/or near the bottom of the strongly layered zone (Fig. 3C). Described by Taner et al. (1998), the magnetite horizon is characterized by strongly layered to massive, medium- to coarse-grained magnetite. In polished section and hand specimen, the magnetite shows a well-annealed (tight, mosaic) granular texture, suggestive of a very low permeability ($<10^{-18}$ m^2: Oelkers, 1996) similar to magnetite-rich layers from the Bushveld Complex, South Africa (Reynolds, 1985a, b). Confined to the strongly layered zone, the hydrothermal cracking zone apparently did not penetrate into and/or below the magnetite horizon, suggesting that the magnetite horizon may have acted as a lower, higher tensile strength boundary for the hydrothermal cracking zone and hydrothermal fluid penetration in general. Such a boundary is consistent with work by Lister (1982) that suggests the penetration of hydrothermal cracking can be stalled or halted by a change in the tensile strength of the host rock.

Cathles (1993) described a conductive thermal-boundary layer that separates hot (1,200°C) magma below from cooler (350°C) convecting hydrothermal fluids above. Numerical modeling by Lowell and Rona (1985), Cann et al. (1985), Lowell and Burnell (1991), and Cathles (1993) has shown that heat output from black smokers can be maintained only if the conductive thermal-boundary layer remains thin (<~180 m: Cathles, 1993). Based on field relationships, we suggest that the magnetite horizon at Matagami may represent the top of the conductive thermal boundary layer. This interpretation in

turn suggests that magma existed within the Bell River Complex ~1,200 to 1,500 m below the top of the intrusion (2,200–2,500 m beneath the paleosea floor) at the time of VMS formation. This depth approximately corresponds to the contact between the Layered and the Main zones of the Bell River Complex (Figs. 6, 8). The relatively high thermal conductivity (1.7 $Wm^{-1}K^{-1}$ at ~600°–800°C) and cold crushing strength (35–60 MPa) of magnetite are consistent with the proposed association of the magnetite horizon with the thermal-boundary layer.

The dominant orientation of quartz-epidote veins parallels the orientation of the primary layering. This is illustrated in Figures 9 and 10 and is also apparent from the orientation of the calculated permeability tensors (Fig. 5A). Horizontal fractures are ideal for fluid phase separation (Norton and Knight, 1977; Hardee, 1982; Delaney et al., 1987), suggesting that, all other considerations aside, the geometry of the hydrothermal cracking zone at Matagami may have favored or enhanced the production of highly saline brines (38.2 ± 1.9 wt % NaCl equiv) deep within the hydrothermal system (Ioannou et al., 2007). Furthermore, phase separation itself may have played a direct role in the creation of the horizontal cracks, as P_{fluid} exceeded $P_{lithostatic}$ within the Bell River Complex during hydrothermal fluid invasion (Ioannou et al., 2007). This situation is similar to the creation of closely spaced fractures in porphyry-type systems when P_{fluid} exceeds $P_{lithostatic}$ (Burnham and Ohmoto, 1980, 1981).

In the simplest case, parallelism of fractures and layering may occur as downwelling fluids are drawn toward the intrusive heat source and are heated while traveling parallel to the outer contact of the intrusion (Kelley and Delaney, 1987; Rosenberg et al., 1993). At Matagami, the sill-like geometry of the Bell River Complex implies a horizontal flow path within the intrusion at most locations. Once the fluid is significantly heated, buoyant forces carry it along steeper, subvertical conduits (localized, see below) toward the sea floor. The overall cycle is analogous to the simple single-pass models of Lowell and Germanovich (1994). In addition, the heterogeneities associated with the layer contacts may have provided planes of low tensile strength along which the hydrothermal cracks preferentially developed (Gudmundsson et al., 2002). Such an interpretation further explains why the hydrothermal cracking zone appears to be concentrated in the strongly layered zone; where there are many more planes of heterogeneity. A similar structural fabric control on fracture orientation has been documented in the sheeted dike complex of the Troodos ophiolite where quartz-epidote veins, a product of on-axis hydrothermal circulation, are preferentially oriented parallel to the plane of the dikes producing an anisotropic permeability (van Everdingen, 1995).

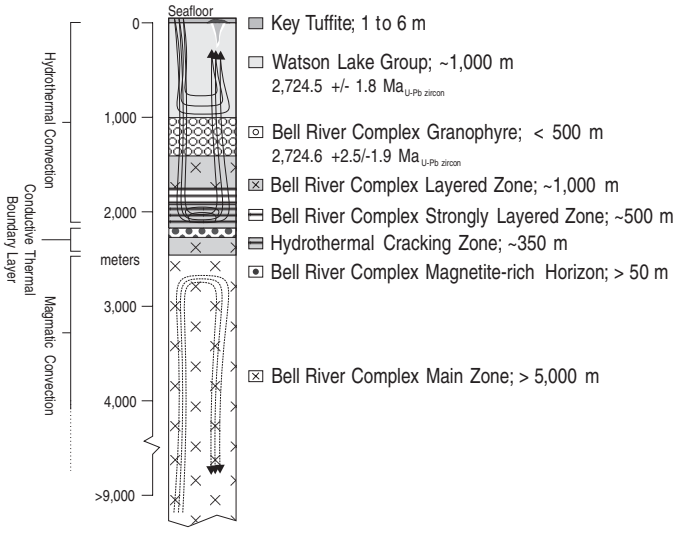

FIG. 8. Schematic stratigraphic section of the Bell River Complex, showing the locations of suggested hydrothermal and magmatic convection during the time of VMS formation.

In addition to fracturing parallel to layering, local zones of quartz-epidote veining approximately orthogonal to layering also occur. The orthogonal veins are usually less continuous and commonly truncated, but not crosscut, by layer parallel veins (Fig. 9). The orthogonal subset of veins is interpreted to represent short pathways that allowed fluids to travel between adjacent layer-parallel vein sets. These orthogonal pathways likely developed in localized zones of structural disturbance that created weaknesses normal to the planes of layering. Such disturbances may have been associated with an extensional sea-floor tectonic regime or sea-floor doming associated with the intrusion of the Bell River Complex at the time of VMS deposition. This extensional regime is indicated by local layer-orthogonal veins that are significantly more continuous, spanning the entire length (±20 m) of an outcrop. These longer vein structures show normal offsets of layering of 10 to 30 cm (Fig. 3D), are broadly spaced along the hydrothermal cracking zone (10- to 30-m spacing inferred from limited outcrop exposure), and are interpreted to represent the initial pathways that allowed fluids to exit the Bell River Complex hydrothermal cracking zone, enter the overlying stratigraphy, and subsequently deposit their metals on the sea floor. For example, the orientations of well-developed layer-orthogonal veins exposed within the western part of the town of Matagami are aligned with the inferred upflow for the Bell Channel VMS deposit directly to the north (Fig. 6). A set of parallel open cracks with apertures of 3 mm, regularly spaced at 20 m, generates a high permeability of 10^{-10} m^2 (using the relationship of Snow, 1965, 1968, 1970).

The less pronounced layer-parallel orientations and the general lack of layer-orthogonal orientations in the high-temperature vein set are likely attributable to the higher temperature of the intrusion, and thus more plastic behavior, and the lower amount of thermal contraction during the times these veins were formed (Cathles, 1993; Barrie et al., 1999).

Similar relationships, in which hydrothermal cracking is confined to the strongly layered zone of the upper Bell River Complex, also occur at the Cold Spring and Des Isles Rapids areas (Fig. 2). However, both approximately layer-parallel and layer-orthogonal quartz-epidote vein orientations occur with similar frequencies, as is evident from the orientation of the calculated permeability tensors (Fig. 5C, E). Such vein orientations suggest that both the Cold Spring and Des Isles Rapids areas investigated are more typical of localized layer-orthogonal flow zones. Structural disturbances, in the form of faulting and layer slumping, are more abundant in these areas than in the town of Matagami. Also, because of a lack of outcrop, the scale

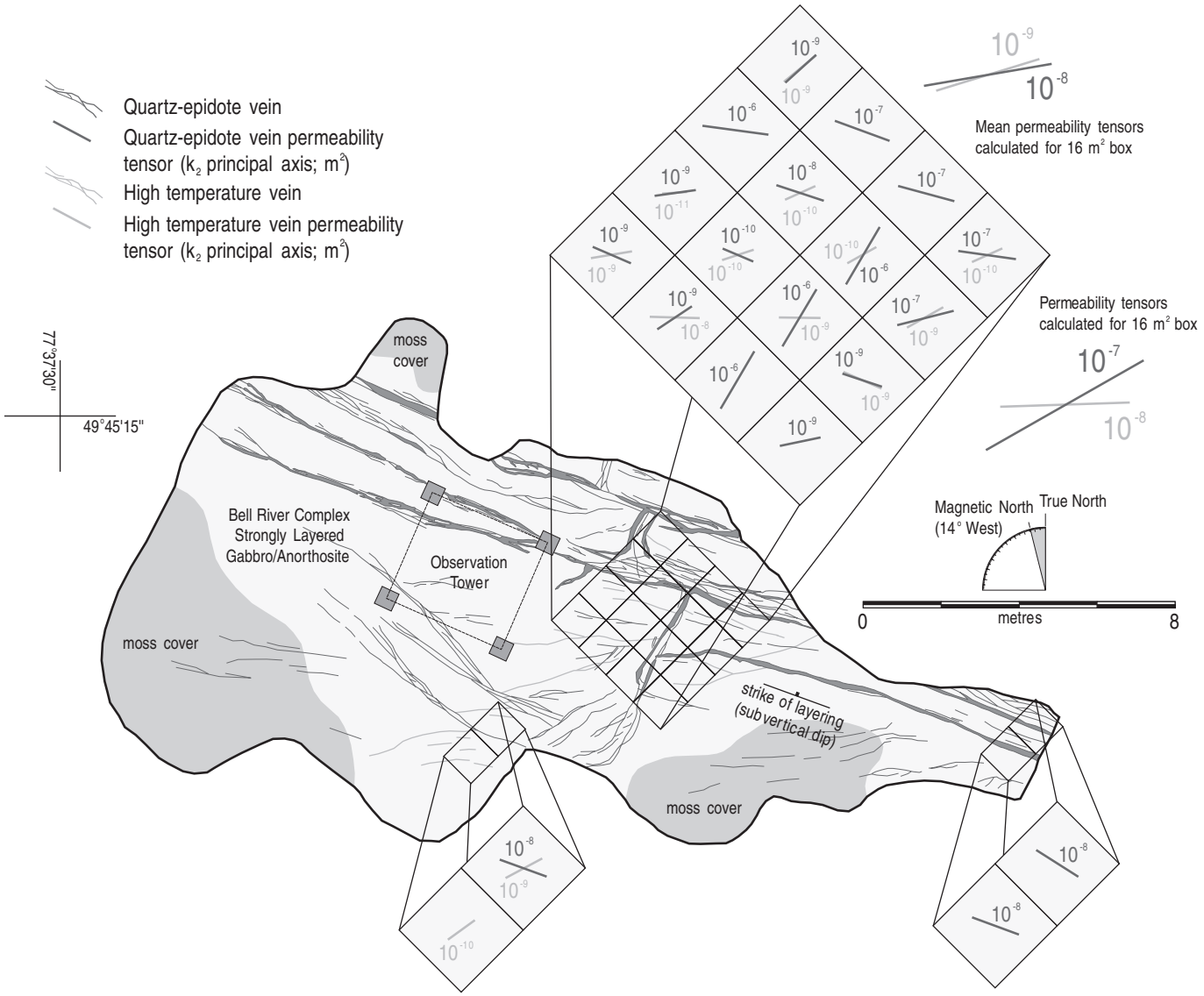

FIG. 9. Permeability tensor data for the 16-m^2 megaframe, Matagami, Quebec (see Fig. 7 for location).

of the Cold Spring and Des Isles Rapids areas investigated is significantly smaller than the broad zone of hydrothermal cracking measured and mapped near the town of Matagami.

During mapping, an effort was made to locate quartz-epidote and high-temperature veins, similar to those of the hydrothermal cracking zone, in the overlying Watson Lake Group volcanics. However, no such veins were found, which supports our interpretation that fluids heated within the hydrothermal cracking zone subsequently underwent focused discharge onto and/or near the sea floor along widely spaced first-order structures which are difficult to locate. MacGeehan (1978) does note the presence of quartz-epidote veins oriented parallel to stratigraphy in B3 basalts (Wabassee Group) along the north limb. However, these vein sets are of considerably smaller scale and likely represent convective circulation pathways associated with the localized intrusion of gabbro sills into the water-saturated pillow basalts as originally proposed by MacGeehan (1978).

Distinct recharge pathways that would have allowed seawater to circulate into the hydrothermal cracking zone of the Bell River Complex were not located during mapping. However, we emphasize the relatively poor outcrop exposure and do not discount that such pathways, likely first-order structures, existed during the Archean.

Permeability distribution

As expected, the maximum model permeability of the hydrothermal cracking zone varies by several orders of magnitude from location to location, both regionally and locally. From a large-scale perspective (Fig. 7), the hydrothermal cracking zone clearly runs subparallel to Bell River Complex stratigraphy and contains mappable, semicontinuous zones of varying permeability. However, it does migrate somewhat vertically relative to the magnetite horizon.

The magnitude of permeability appears to increase toward the center of the hydrothermal cracking zone where it has a

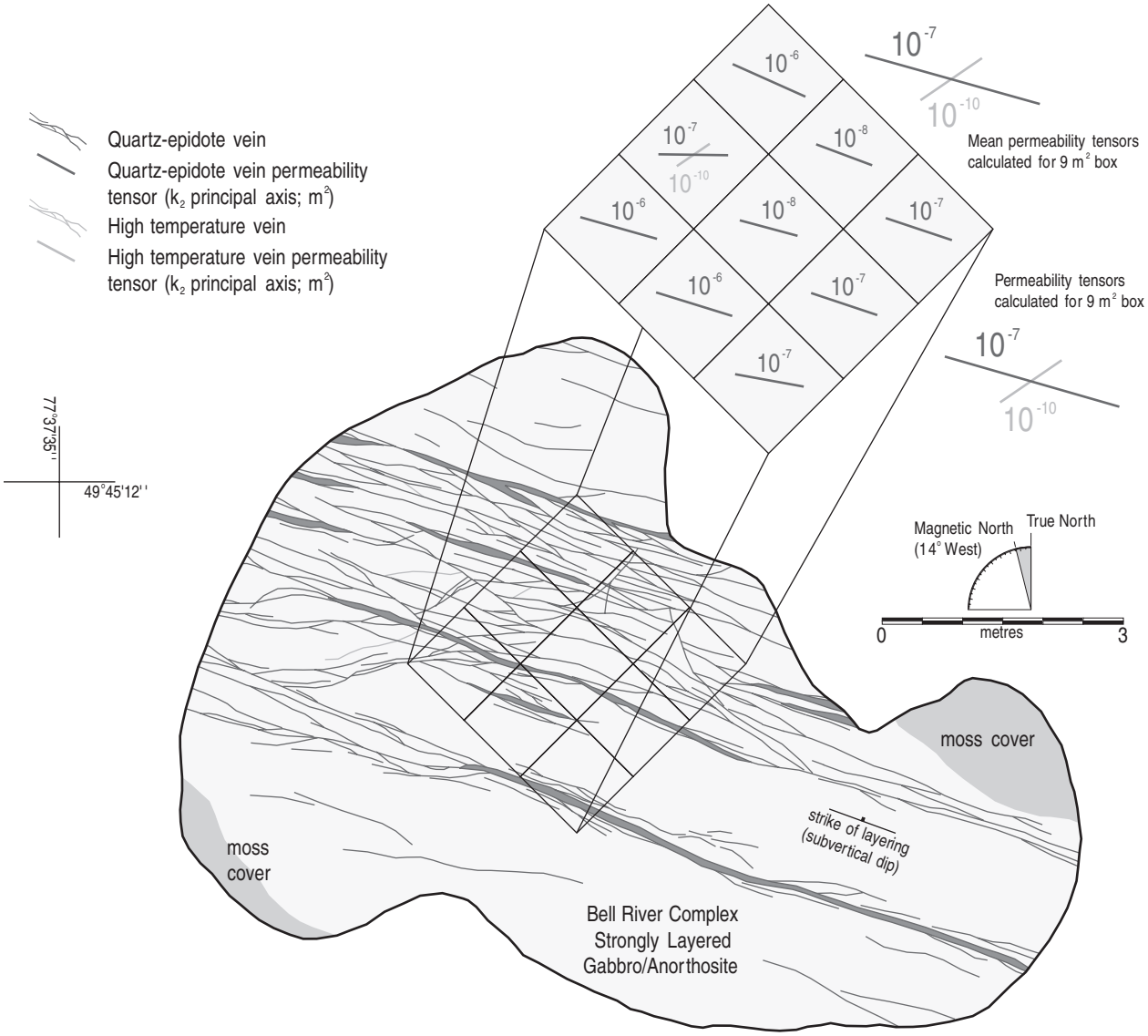

FIG. 10. Permeability tensor data for the 9-m^2 megaframe, Matagami, Quebec (see Fig. 7 for location).

value of approximately 10^{-7} m^2. The common occurrence of approximately two to five veins per m^2 with apertures in excess of 2 cm in this high-flow zone results in localized maximum model permeabilities as high as 10^{-6} to 10^{-5} m^2. The stability of such large aperture openings in the hydrothermal cracking zone is questionable, and excluding these veins from any given sample site decreases the calculated maximum model permeability by ~two orders of magnitude. Rock outside the ~350-m-thick hydrothermal cracking zone is essentially devoid of any veining typical of the hydrothermal cracking zone, thus limiting permeability to low values.

The well-defined boundaries of the hydrothermal cracking zone at Matagami support Cathles' (1993) model, which suggests that cracking develops over discrete and well-constrained zones. Cathles' (1993) model predicts a significantly thinner zone of hydrothermal cracking of only ~3 m at any given time. However, he envisioned a dynamic front sweeping back and forth across stratigraphy in response to changes in the thermal regime of the hot (~1,200°C) intrusion (e.g., phases of cooling or fresh magma injection: Maier et al., 1996), eventually cracking rock over significant intervals, potentially 350 m thick, as at Matagami. The sweeping action of such a front may explain why the central portions of the hydrothermal cracking zone record the highest permeability; central parts are subject to more frequent cracking events as the front traverses back and forth. Furthermore, a lack of crosscutting relationships within the quartz-epidote vein set suggests that repeated fracturing of specific volumes within the hydrothermal cracking zone not only created new fractures for fluid transport but also reactivated old ones, ultimately creating the localized zones of very high (>10^{-8} m^2) maximum model permeability observed in this study.

It should be noted that Cathles' (1993) models are based on intrusions with dikelike geometries, with the thickness of the hydrothermal cracking zone proportional to the surface area of the flow zone facing the magma chamber. Therefore, the

sill-like geometry of the Bell River Complex may account, at least in part, for the significantly thicker hydrothermal cracking zone of 350 m, as opposed to ~3 m, as discussed by Cathles (1993). Intrusion geometry has been shown to affect hydrothermal circulation pathways (e.g., Solomon et. al., 1987; Brikowski and Norton, 1989) and further study is needed to investigate the effects of intrusion geometry on the numerically derived thickness of the hydrothermal cracking zone. At Matagami, folding and erosion have distorted the geometry of the Bell River Complex, making the use of numerical methods to calculate a thickness of the hydrothermal cracking zone difficult.

Quartz-epidote veining and high-temperature veining occur together in and around the town of Matagami, although the former is more prominent. However, at Cold Spring Rapids and to a lesser extent at Des Isles Rapids, discrete, moderate- to high-density (20–45 veins/m^2) quartz-epidote and high-temperature (magnetite-rich) vein-dominant zones occur separately. Hydrothermal cracking between these two zones, spaced up to 200 m apart, is poorly to moderately developed and defined by sparse (<10 veins/m^2) quartz-epidote–dominant veining. In this case, spatial segregation of the cracking zones supports a (locally) mobile front capable of changing position up to a few hundred meters over time, assuming the high-temperature veins are the product of earlier stage higher temperature cracking events as suggested in the model of Cathles (1993).

Toward the eastern end of the map area (Figs. 6, 7), the hydrothermal cracking zone appears to bifurcate. This is not unexpected, as particular zones within the strongly layered zone develop cracks, which are amplified with subsequent cooling. Mapping along the eastern shoreline of the Bell River indicates that either the two bifurcated arms of the hydrothermal cracking zone rejoin or one is terminated somewhere beneath Bell River, suggesting that bifurcation may have been the result of crack development in particular preferred zones separated by a less preferred zone.

In moderate- to low-flow zones within the hydrothermal cracking zone, where vein densities are low yet generally consistent, a 1-m^2 frame positioned in a fractured zone representative of an entire outcrop and/or area is effective at characterizing the permeability of that area. However, in high-flow zones (>25 veins/m^2), commonly characterized by sudden changes in vein density and aperture associated with complex branching and/or convergence, the 1-m^2 frames produce tensor data that reflects the significant variation in permeability that can occur over short distances. Order of magnitude changes in permeability are not uncommon between frames directly adjacent to each other; in extreme cases, differences of up to three orders of magnitude can occur (>10^{-5} to <10^{-11} m^2: Figs. 9, 10). These large variations over very short distances make it difficult to characterize accurately the permeability of an overall high-flow zone using a 1-m^2 frame.

At two specific outcrops where good high-flow zone exposure was available over a significant area, multiple frames were measured directly adjacent to each other along a grid-like pattern, thereby producing "megaframes" covering 9 and 16 m^2 (Figs. 9, 10), thus taking into account the heterogeneity between the 1-m^2 frames and producing a more representative permeability tensor for an area and/or outcrop as a whole. A permeability of ~10^{-7} m^2 for a quartz-epidote vein system measured at this scale likely represents a good first-order estimate of the maximum permeability that can be expected over any significant high-flow zone volume within the hydrothermal cracking zone.

Modeling by Cathles (1993) predicts a 330-milliDarcy (3.3×10^{-13} m^2) permeability for the hydrothermal cracking zone around midocean ridge intrusions; low compared to the data presented here. However, Cathles noted that minor increases in flow porosity, for example, induced by episodes of magma-chamber deflation associated with volcanism or by thermal contraction of the thermal-boundary layer, can increase permeability by factors >>10^3.

Given a thermal contraction coefficient of 3.3×10^{-5} °C^{-1}, thermal contraction associated with cooling from 1,200° to 350°C will result in the creation of 3.5 percent fracture porosity (Cathles, 1993). At Matagami, an average fracture aperture of 1 mm and average vein density of 15 veins per m^3, the lower values characteristic for quartz-epidote veins, produces an effective porosity of 1.5 percent; a porosity attainable through thermal contraction alone. However, an average fracture aperture of 3 mm and average vein density of 25 veins per m^3, which are the upper values characteristic for quartz-epidote veins, produces an effective porosity of 7.5 percent, suggesting that additional processes may be contributing to the creation of fracture porosity in the Bell River Complex hydrothermal cracking zone. Thermal contraction of the thermal-boundary layer at Matagami is supported by fluid inclusion data, which indicate that the fluids in the quartz-epidote veins of the Bell River Complex were highly saline (38.2 ± 1.9 wt % NaCl equiv; Ioannou et al., 2007), a result of phase separation possibly along cracks extending into the thermal-boundary layer (cf. Cathles, 1993). Phase separation itself is accompanied by an increase in volume. Hence, the Bell River Complex hydrothermal cracking zone may have been amplified by hydraulic cracking and volumetric expansion similar to fracturing processes associated with copper porphyry deposits (Fournier, 1999; Tosdal and Richards, 2001). A >10^3 increase in the permeability value proposed by Cathles (1993) is in reasonable agreement with permeability tensor magnitudes, representative of the (bulk) hydrothermal cracking zone, calculated here (10^{-10}–10^{-8} m^2; not counting localized high-flow zones). Likewise, reasonable agreement between field measurements (Nehlig and Juteau, 1988; van Everdingen, 1995; this study) and theoretically based (Cathles, 1993; Fisher and Becker, 1995) permeability data further supports the interpretation that quartz-epidote veining in the strongly layered zone of the Bell River Complex is a product of hydrothermal cracking (Table 2).

In situ bulk permeability measurements obtained from the modern ocean floor vary by six orders of magnitude, from 10^{-18} to 10^{-12} m^2 (e.g., Becker, 1989, 1991) and are lower than the values calculated here for the permeability of the hydrothermal cracking zone (Table 3). Of all the holes drilled by the Ocean Drilling Program, only ODP hole 504B penetrates deep below the sea floor into layer 2B sheeted dikes of the oceanic crust (up to 1,600 m: Becker, 1989). Permeabilities determined from in situ packer injection tests in hole 504B sheeted dikes are approximately 10^{-18} to 10^{-17} m^2; the 20- to 50-m scale of such subsea-floor packer injection tests is of a

TABLE 3. Examples of In Situ Measured Permeability from the Modern Sea Floor

Site	k (m^2)	Temperature (°C)	mbsf/*mbbt*[1]	k measurement technique	References	Notes
Hole 395A	10^{-14}–10^{-13}	3 - 9	*100 – 350*	Downhole temperature logging	Kopietz et al. (1990)	Layer 2A - pillow lavas; 110 km off axis (Mid Atlantic Ridge) in 7 Ma crust
Hole 395A	10^{-14}	6–19	396–606	Drill-string packer injection	Becker (1990); Kopietz et al. (1990)	Layer 2A - pillow lavas; 110 km off axis (Mid Atlantic Ridge) in 7 Ma crust
Hole 395A	10^{-18}–10^{-17}	16–19	583–664 490–571	Drill-string packer injection	Hickman et al. (1984); Kopietz et al. (1990)	Layer 2A - pillow lavas (low k zone); 110 km off axis (Mid Atlantic Ridge) in 7 Ma crust
Hole 504B	$> 6 \times 10^{-14}$	5–70	274.5–374.5 0–100	Downhole temperature logging	Becker et al. (1983) Guerin et al. (1996)	Layer 2A - pillow lavas; 200 km off axis (Costa Rica rift) in 6 Ma crust
Hole 504B	10^{-14}–10^{-13}	5–80	*0–150*	Drill-string packer injection	Becker et al. (1983); Anderson et al. (1985) Guerin et al. (1996	Layer 2A - pillow lavas; 200 km off axis (Costa Rica rift) in 6 Ma crust
Hole 504B	10^{-17}	>120	*>550*	Drill-string packer injection	Becker et al. (1983); Anderson et al. (1985) Guerin et al. (1996	Layer 2A - pillow lavas; 200 km off axis (Costa Rica rift) in 6 Ma crust
Hole 504B	10^{-18}–10^{-17}	130–170	900–1,600	Drill-string packer injection	Becker et al. (1983); Becker (1989) Guerin et al. (1996)	Layer 2B - sheeted dike complex; 200 km off axis (Costa Rica rift) in 6 Ma crust
Hole 735B	10^{-16}–10^{-12}	>9	350–800	Drill-string packer injection	Becker (1991); Von Herzen and Scott (1991)	Layer 3 - gabbro; 18 km off axis axis (Southeast Indian Ridge) in 12 Ma crust
Hole 839B	$1–5 \times 10^{-12}$	na	398.2	Drill-string packer injection	Bruns and Lavoie (1994)	Layer 2A - pilow lavas; (Lau basin) in < 6 Ma crust
Hole 896A	10^{-13}	10	195–233 16–54	Drill-string packer injection	Becker (1996)	Layer 2A - pillow lavas; 200 km off axis (Costa Rica rift) in 6 Ma crust
Hole 896A	10^{-14}	20	233–469 54–290	Drill-string packer injection	Becker (1996)	Layer 2A - pillow lavas; 200 km off axis (Costa Rica rift) in 6 Ma crust

[1] mbsf = meters below sea floor, mbbt = meters below basement top (italics)

similar scale to the outcrop fracture mapping done for this study. Hole 504B permeability values are also considerably lower than values obtained from field-based fracture measurements from the sheeted dikes of the Omai and Troodos ophiolites, which yield permeabilities of 10^{-12} to 10^{-6} m^2 (Nehlig and Juteau, 1988; van Everdingen, 1995), and are more consistent with values from this study (Table 2). However, hole 504B was drilled 200 km off the Costa Rica Ridge axis in 6 Ma crust and therefore does not likely preserve the permeability structure of the sheeted dike complex during on-axis hydrothermal circulation. The permeability of the sheeted dike complex decreases through time as fractures become filled with minerals deposited by circulating hydrothermal fluids. Circulation of cooler, calcite and/or lower temperature clay precipitating fluids off-axis may subsequently occur under very low permeability conditions (e.g., $k = 10^{-20}$–10^{-18} m^2; Becker, 1989; van Everdingen, 1995). The permeability difference between Bell River Complex hydrothermal cracking zone and bulk off-axis oceanic crust discussed above highlights the importance of recognizing physical macroscopic features of the hydrothermal cracking zone. Although volumetrically small in comparison with the permeability structure of the bulk sea floor, the significantly higher permeability of the hydrothermal cracking zone controlled fluid flow deep within the hydrothermal system.

Conclusions

Detailed field measurements of quartz-epidote and high-temperature vein geometries coupled with permeability tensor theory have produced a first-order approximation of the permeability structure of the hydrothermal cracking zone exposed in the Matagami VMS district, Quebec. Representative district-wide values indicate a maximum bulk model permeability of 10^{-10} to 10^{-8} m^2 for the hydrothermal cracking zone. However, a high-flow zone located within the central parts of the hydrothermal cracking zone is characterized by a maximum model permeability of 10^{-7} m^2. On a more local scale (<1 m^2), the high-flow zone reaches maximum model permeability values as high as 10^{-6} to 10^{-5} m^2 where two or more veins occur with apertures in excess of 2 cm.

Field mapping has shown that the hydrothermal cracking zone is confined to a ~350-m-thick interval located within strongly layered gabbro and/or anorthosite of the Layered zone, upper Bell River Complex. The base of this interval is

located 1,000 m below the top of the Bell River Complex. Furthermore, in and around the town of Matagami, the dominant orientation of quartz-epidote veins parallels the orientation of the layering (110° ± 15°). This is further reflected in the orientation of the calculated permeability tensors of the quartz-epidote veins (94° ± 30°, 1σ, n = 71). The layer-parallel fracturing suggests that heterogeneities associated with the layer contacts provided planes of low tensile strength along which the hydrothermal cracks preferentially developed. Such an interpretation further explains why the hydrothermal cracking zone appears to be restricted to the strongly layered zone where there are many more planes of heterogeneity.

Local zones of quartz-epidote veining approximately orthogonal to layering are also present. The orthogonal veins are typically less continuous and commonly truncated (but not crosscut) by layer-parallel veins. The orthogonal subset of veins is interpreted to represent short pathways that allowed fluids to travel between adjacent layer-parallel veins. Locally, longer layer-orthogonal quartz-epidote veins offset layering in the Bell River Complex by 10 to 30 cm and may represent initial conduits that allowed fluids to travel into overlying stratigraphy. The less pronounced layer-parallel veins and the general lack of layer-orthogonal orientations in the high-temperature vein set are likely attributable to the higher temperature of the intrusion and thus more plastic behavior and lower amount of thermal contraction during the times these veins were formed.

Although volumetrically small in comparison with the permeability structure of the bulk sea floor, the significantly higher permeability of the hydrothermal cracking zone indicates its importance in controlling the flow paths and fluxes of fluids deep within the hydrothermal system. As demonstrated here, tensor theory is a powerful tool that can be used to calculate meaningful, first-order estimates of both bulk and end-member permeabilities for preserved hydrothermal systems. Such estimates, based on field data, are critical input and/or testing parameters for subsequent fluid-flow model calculations.

Acknowledgments

We thank Grant Arnold and Noranda Inc. for their logistical support during the acquisition of field data from the Matagami district. Dominic Bruscia's help during the collection of field measurements during summer 2000 is greatly appreciated. Funding for this research was provided by NSERC (File 661-069-97 and a PGS-B scholarship), CAMIRO (Project 96E01), the Ontario Government Graduate Scholarship (OGS and OGSST) program, and the Department of Geology, University of Toronto (Steven D. Scott, Chair). We also thank C. Tucker Barrie and Richard C. Bailey for their insight and practical support throughout this study. *Economic Geology* reviewers Kathy Gillis, Masanobu Oda, John Dilles, and Mark Hannington provided constructive input that benefited this manuscript.

February 20, 2004; July 18, 2007

REFERENCES

Alt, J.C., 1995, Subseafloor processes in mid-ocean ridge hydrothermal systems: Geophysical Monograph 91, p. 85–114.

Anderson, R.N., Zoback, M.D., Hickman, S.H., and Newmark, R.L., 1985, Permeability versus depth in the upper oceanic crust: In situ measurements in deep sea drilling project hole 504B, eastern equatorial Pacific: Initial Reports of the Deep Sea Drilling Project, v. 83, p. 429–442.

Barrie, C.T., Cathles, L.M., and Erendi, A., 1999, Finite element heat and fluid-flow computer simulations of a deep ultramafic sill model for the giant Kidd Creek volcanic-associated massive sulfide deposit, Abitibi subprovince, Canada: Economic Geology Monograph 10, p. 529–540.

Beaudry, C., and Gaucher, E., 1986, Cartographie géologique dans la région de Matagami: Québec Ministère de l'Energie et des Ressources Report MB 86–32, 147 p.

Becker, K., 1989, Measurements of the permeability of the sheeted dikes in hole 504B ODP Leg 111: Proceedings of the Ocean Drilling Program, Scientific Results, v. 111, p. 317–355.

——1990, Measurements of the permeability of the upper oceanic crust at hole 395A, ODP Leg 109: Proceedings of the Ocean Drilling Program, Scientific Results, v. 106/109, p. 213–222.

——1991, In-situ bulk permeability of oceanic gabbros in hole 735B, ODP leg 118: Proceedings of the Ocean Drilling Program, Scientific Results, v. 118, p. 333–347.

——1996, Permeability measurements in hole 896A and implications for the lateral variability of upper crustal permeability at sites 504 and 896: Proceedings of the Ocean Drilling Program, Scientific Results, v. 148, p. 353–363.

Becker, K., Langseth, M.G., Von Herzen, R.P., and Anderson, R.N., 1983, Deep crustal geothermal measurements, hole 504B, Costa Rica rift: Journal of Geophysical Research, v. 88, p. 3447–3457.

Bianchi, L., and Snow, D.T., 1969, Permeability of crystalline rock interpreted from measured orientations and apertures of fractures: Annual Arid Zone, v. 8, p. 231–245.

Björnsson, H., Björnsson, S., and Sigurgeirsson, T., 1982, Penetration of water into hot rock boundaries of magma at Grímsvötn: Nature, v. 295, p. 580–581.

Bodvarsson, G.S., 1982, Mathematical modeling of the behavior of geothermal systems under exploitation: Unpublished Ph.D. thesis, Berkeley, California, University of California, 353 p.

Borisenko, A.I., and Tarapov, I.E., 1968, Vector and tensor analysis with applications: New York, Dover Publications, p. 109–120.

Brace, W.F., 1980, Permeability of crystalline and argillaceous rocks: International Journal of Rock Mechanics, v. 17, p. 241–251.

Brantley, S.L., Evans, B., Hickman, S.H., and Crerar, D.A., 1990, Healing of microcracks in quartz—implications for fluid flow: Geology, v. 18, p. 136–139.

Brikowski, T, and Norton, D., 1989, Influence of magma chamber geometry on hydrothermal activity at mid-ocean ridges: Earth and Planetary Science Letters, v. 93, p. 241–255.

Brown, S.R., 1987, Fluid flow through rock joints: The effects of surface roughness: Journal of Geophysical Research, v. 92, p. 1337–1347.

Bruns, T.R., and Lavoie, D., 1994, Bulk permeability of young backarc basalt in the Lau basin from a downhole packer experiment (hole 839B): Proceedings of the Ocean Drilling Program, Scientific Results, v. 135, p. 805–816.

Burnham, C.W. and Ohmoto, H., 1980, Late-stage processes of felsic magmatism: Mining Geology Special Issue 8, p. 1–12.

——1981, Late magmatic and hydrothermal processes in ore formation: Mineral Resources: Genetic Understanding for Practical Applications: National Academy Press, Washington, p. 62–72.

Cann, J.R., Strens, M.R., and Rice, A., 1985, A simple magma-driven thermal balance model for the formation of volcanogenic massive sulphides: Earth and Planetary Science Letters, v. 76, p. 123–134.

Carr, P.M., 2004, Physical and chemical consequences of the cooling of sills by pore water convection with application to massive sulfide deposits: Unpublished Ph.D. thesis, Ithaca, New York, Cornell University, 130 p.

Cathles, L.M., 1981, Fluid flow and genesis of hydrothermal ore deposits: Economic Geology 75th Anniversary Volume, p. 424–457.

——1983, An analysis of the hydrothermal system responsible for massive sulfide deposition in the Hokuroku basin of Japan: Economic Geology Monograph 5, p. 439–487.

——1993, A capless 350°C flow zone model to explain megaplumes, salinity variations, and high temperature veins in ridge axis hydrothermal systems: Economic Geology, v. 88, p. 1977–1988.

Cox, S.F., Knackstedt, M.A., and Braun, J., 2001, Principles of structural control on permeability and fluid flow in hydrothermal systems: Reviews in Economic Geology v. 14, p. 1–24.

Davidson, A.J., 1977, Petrography and chemistry of the Key Tuffite at Bell Allard, Matagami, Quebec: Unpublished M.Sc. thesis, Montreal, Quebec,McGill University, 83 p.

de Ronde, C.E.J., 1995, Fluid chemistry and isotopic characteristics of seafloor hydrothermal systems and associated VMS deposits: Potential for magmatic contributions: Mineralogical Association of Canada Short Course, v. 23, p. 479–510.

Delaney. J.R., Mogk, D.W., and Mottl, M.J., 1987, Quartz-cemented breccias from the Mid-Atlantic Ridge: Samples of a high-salinity hydrothermal upflow zone: Journal of Geophysical Research, v. 92, p. 9175–9192.

Dilles, J.H, and Einaudi, M.T., 1992, Wall-rock alteration and hydrothermal flow paths about the Ann-Mason porphyry copper deposit, Nevada: A 6-km vertical reconstruction: Economic Geology, v. 87, p. 1963–2001.

Dilles, J.H., Solomon, G.C., Taylor, H.P., Jr., and Einaudi, M.T., 1992, Oxygen and hydrogen isotope characteristics of hydrothermal alteration at the Ann-Mason porphyry copper deposit, Yerington, Nevada: Economic Geology, v. 87, p. 44–63.

Fisher, A.T., 1998, Permeability within basaltic oceanic crust: Reviews of Geophysics, v. 36, p. 143–182.

Fisher A.T., and Becker, K., 1995, Correlation between seafloor heat flow and basement relief: Observational and numerical examples and implications for upper crustal permeability: Journal of Geophysical Research, v. 100, p. 12,641–12,657.

Fournier, R.O., 1987, Conceptual models of brine evolution in magmatic hydrothermal systems: U.S. Geological Survey Professional Paper 1350, p. 1487–1506.

——1988, Accumulation of thin subhorizontal bodies of fluid in quasi-plastic crystalline rocks at temperatures exceeding 350–400°C: EOS, Transactions of the American Geophysical Union, v. 69, p. 478.

——1999, Hydrothermal processes related to movement of fluid from plastic into brittle rock in the magmatic-epithermal environment: Economic Geology, v. 94, p. 1193–1212.

Freeman, B.C., 1939, The Bell River Complex, northwestern Quebec: Journal of Geology, v. 47, p. 27–46.

Gale, J.E., 1982, The effects of fracture type (induced versus natural) on the stress-fracture closure-fracture permeability relationships: 23rd U.S. Rock Mechanics Symposium, 23rd, Berkeley, California, Proceedings p. 290–298.

Gale, J.E., and Rouleau, A., 1985, Hydrogeological characterization of the ventilation drift area: Information Symposium on In Situ Experiments in Granite Associated with the Disposal of Radioactive Waste, Nuclear Energy Agency, Stockholm, Sweden.

Galley, A.R., Jonasson, I.R., and Watkinson, D.H., 2000a, Magnetite-rich calc-silicate alteration in relation to synvolcanic intrusion at the Ansil volcanogenic massive sulfide deposit, Rouyn-Noranda, Quebec, Canada: Mineralium Deposita, v. 35, p. 619–637.

Galley, A.R., van Breeman, O., and Franklin, J., 2000b, The relationship between intrusion-hosted Cu-Mo mineralization and the VMS deposits of the Archean Sturgeon Lake mining camp, northwestern Ontario: Economic Geology, v. 95, p. 1543–1550.

Gillis, K.M., 1995, Controls on hydrothermal alteration in a section of fast-spreading oceanic crust: Earth and Planetary Science Letters, v. 134, p. 473–489.

Gillis, K.M., and Roberts, M.D., 1999, Cracking at the magma-hydrothermal transition: Evidence from the Troodos Ophiolite, Cyprus: Earth and Planetary Science Letters, v. 169, p. 227–244.

Gudmundsson, A., Fjeldskaar, I., and Brenner, S.L., 2002, Propagation pathways and fluid transport of hydrofractures in jointed and layered rocks of geothermal fields: Journal of Volcanology and Geothermal Research, v. 116, p. 257–278.

Guerin, G., Becker, K., Gable, R., and Pezard, P., 1996, Temperature measurements and heat-flow analysis in hole 504B: Proceedings of the Ocean Drilling Program, Scientific Results, v. 148, p. 291–296.

Hardee, H.C., 1982, Permeable convection above magma bodies: Tectonophysics, v. 84, p. 179–195.

Harper, G.D., 1999, Structural styles of hydrothermal discharge in ophiolite/sea-floor systems: Reviews in Economic Geology, v. 8, p. 53–73.

Haynes, F.M., and Titley, S.R., 1980, The evolution of fracture-related permeability within the Ruby Star Granodiorite, Sierrita porphyry copper deposit, Pima County, Arizona: Economic Geology, v. 75, p. 673–683.

Hickman, S.H., Langseth, M.G., and Svitek, J.F., 1984, In situ permeability and pore-pressure measurements near the Mid-Atlantic Ridge, deep sea drilling project hole 395A: Initial Results of the Deep Sea Drilling Project, v. 78B, p. 699–708.

Ioannou, S.E., 2004, Hydrothermal fluid chemistry and flow paths associated with the Archean Matagami VMS system, Abitibi subprovince, Canada: Unpublished Ph.D. thesis, Toronto, Ontario, University of Toronto, 275 p.

Ioannou, S.E., Götze, J., Weiershäuser, L., Zubowski, S.M., and E.T.C. Spooner, 2004, Cathodoluminescence characteristics of Archean VMS-related quartz: Noranda, Ben Nevis and Matagami districts, Abitibi subprovince, Canada: Geochemistry, Geophysics, Geosystems, v. 5, Q02007, doi:10.1029/2003GC000613.

Ioannou, S.E., Spooner, E.T.C., and Barrie, C.T., 2007, Fluid temperature and salinity characteristics of the Matagami volcanogenic massive sulfide district, Quebec: Economic Geology, v. 102, p. 691–715.

Kelley, D.S., and Delaney, J.R., 1987, Two-phase separation and fracturing in mid-ocean ridge gabbros at temperatures greater than 700°C: Earth and Planetary Science Letters, v. 83, p. 53–66.

Kerr, D.J., and Gibson, H.L., 1993, A comparison of the Horne volcanogenic massive sulfide deposit and intracauldron deposits of the Mine sequence, Noranda, Quebec: Economic Geology, v. 88, p. 1419–1442.

Kopietz, J., Becker, K., and Hamano, Y., 1990, Temperature measurements at site 395, ODP Leg 109: Proceedings of the Ocean Drilling Program, Scientific Results, v. 106/109, p. 197–203.

Kristmannsdóttir, H., 1979, Alteration of basaltic rocks by hydrothermal activity at 100–300°C, *in* Mortland, M.M., and Farmer, V.C., eds., International Clay Conference 1978: Amsterdam, Elsevier Scientific Publishing, p. 359–367.

Lacroix, S., Simard, A., Pilote, P., and Dubé, L., 1990, Regional geologic elements and mineral resources of the Harricana-Turgeon belt, Abitibi subprovince of NW Quebec: Canadian Institute of Mining and Metallurgy Special Volume 43, p. 313–326.

Liaghat, S., and MacLean, W.H., 1992, The Key Tuffite, Matagami mining district: Origin of the tuff components and mass changes: Exploration and Mining Geology, v. 1, p. 197–207.

Lister, C.R.B., 1972, On the thermal balance of a mid-ocean ridge: Geophysical Journal of the Royal Astronomical Society, v. 26, p. 515–535.

——1974, On the penetration of water into hot rock: Geophysical Journal of the Royal Astronomical Society, v. 39, p. 465–509.

——1975, Qualitative theory on the deep end of geothermal systems: Second United Nations Symposium on the Development and Use of Geothermal Resources, p. 459–463.

——1982, "Active" and "passive" hydrothermal systems in the oceanic crust: Predicted physical conditions, *in* Fanning, K.A., and Manheim, F.T., eds., The dynamic environment of the ocean floor: Lexington, Massachusetts, Lexington Books, p. 441–470.

——1983, The basic physics of water penetration into hot rocks, *in* Rona, P.A., Bostrom, K., Laubier, L., and Smith, K.L., eds., Hydrothermal processes at seafloor spreading centers, New York, Plenum Press, p. 141–168.

——1986, Differential thermal stress in the earth: Geophysical Journal of the Royal Astronomical Society, v. 86, p. 319–330.

Long, J.C.S., and Witherspoon, P.A., 1985, The relationship of the degree of interconnection to permeability in fracture networks: Journal of Geophysical Research, v. 90, p. 3087–3098.

Long, J.C.S., Remer, J.S., Wilson, C.R., and Witherspoon, P.A., 1982, Porous media equivalents for networks of discontinuous fractures: Water Resources Research, v. 18, p. 645–658.

Lowell, R.P., and Burnell, D.K., 1991, Mathematical modeling of conductive heat transfer from a freezing, convecting magma chamber to a single-pass hydrothermal system: Implications for seafloor black smokers: Earth and Planetary Science Letters, v. 104, p. 59–69.

Lowell, R.P., and Germanovich, L.N., 1994, On the temporal evolution of high-temperature hydrothermal systems at ocean ridge crests: Journal of Geophysical Research, v. 99, p. 565–575.

Lowell, R.P., and Rona, P.A., 1985, Hydrothermal models for the generation of massive sulfide ore deposits: Journal of Geophysical Research, v. 90, p. 8769–8783.

MacGeehan, P.J., 1978, The geochemistry of altered volcanic rocks at Matagami, Quebec: A geothermal model for massive sulphide genesis: Canadian Journal of Earth Sciences, v. 15, p. 551–570.

MacGeehan, P.J., and MacLean, W.H., 1980a, An Archean sub-seafloor geothermal system, "calc-alkali" trends, and massive sulphide genesis: Nature, v. 286, p. 767–771.

——1980b, Tholeiitic basalt-rhyolitic magmatism and massive sulphide deposits at Matagami, Quebec: Nature, v. 283, p. 153–157.

Maier, W.D., Barnes, S.J., and Pellet, T., 1996, The economic significance of the Bell River Complex, Abitibi subprovince, Quebec: Canadian Journal of Earth Sciences, v. 33, p. 967–980.

Manning, C.E., and Bird, D.K., 1986, Hydrothermal clinopyroxenes of the Skaergard intrusion: Contributions to Mineralogy and Petrology, v. 92, p. 437–447.

Manning, C.E., Weston, P.E., and Mahon, K.I., 1996, Rapid high-temperature metamorphism on East Pacific Rise gabbros from Hess Deep: Earth and Planetary Science Letters v. 144, p. 123–132.

Mortensen, J.K., 1993, U-Pb geochronology of the eastern Abitibi subprovince, Part 1: Chibougamau-Matagami-Joutel region: Canadian Journal of Earth Sciences, v. 30, p. 11–28.

Nehlig, P., 1991, Salinity of oceanic hydrothermal fluids: A fluid inclusion study: Earth and Planetary Science Letters, v. 102, p. 310–325.

——1993, Interactions between magma chambers and hydrothermal systems: Oceanic and ophiolitic constraints: Journal of Geophysical Research, v. 98, p. 19621–19633.

——1994, Fracture and permeability analysis in magma-hydrothermal transition zones in the Semail ophiolite (Oman): Journal of Geophysical Research, v. 99, p. 589–601.

Nehlig, P., and Juteau, T., 1988, Flow porosities, permeabilities and preliminary data on fluid inclusions and fossil thermal gradients in the crustal sequence of the Semail ophiolite (Oman): Tectonophysics, v. 151, p. 199–221.

Nehlig, P., Juteau, T., Bendel, V., and Cotton, J., 1994, The root zone of oceanic hydrothermal systems: Constraints from the semail ophiolite (Oman): Journal of Geophysical Research, v. 99, p. 4703–4713.

Nicolas, A., Reuber, I., and Benn, K., 1988, A new magma chamber model based on structural studies in the Oman ophiolite: Tectonophysics, v. 151, p. 87–105.

Norton, D., and Knapp, R., 1977, Transport phenomena in hydrothermal systems: The nature of porosity: American Journal of Science, v. 277, p. 913–936.

Norton, D., and Knight, J., 1977, Transport phenomena in hydrothermal systems: Cooling plutons: American Journal of Science, v. 277, p. 937–981.

Oda, M., 1983, A method for evaluating the effect of crack geometry on the mechanical behavior of cracked rock masses: Mechanics of Materials, v. 2, p. 163–171.

——1984, Similarity rule of crack geometry in statistically homogeneous rock masses: Mechanics of Materials, v. 3, p. 119–129.

——1985, Permeability tensor for discontinuous rock masses: Géotechnique, v. 35, p. 483–495.

——1986, An equivalent continuum model for coupled stress and fluid flow analysis in jointed rock masses: Water Resources Research, v. 22, p. 1845–1856.

Oda, M., Hatsuyama, Y., and Ohnishi, Y., 1987, Numerical experiments on permeability tensor and its application to jointed granite at Stripa mine, Sweden: Journal of Geophysical Research, v. 92, p. 8037–8048.

Oelkers, E.H., 1996, Physical and chemical properties of rocks and fluids for chemical mass transport calculations: Reviews in Mineralogy v. 34, p. 131–191.

Piché, M., Guha, J., Daigneault, R., Sullivan, J.R., and Bouchard, G., 1990, Les gisements volcanogènes du camp minier de Matagami: structure, stratigraphie et implications métallogeniques: Canadian Institute of Mining and Metallurgy Special Volume 43, p. 327–336.

Piché, M., Guha, J., and Daigneault, R., 1993, Stratigraphic and structural aspects of the volcanic rocks of the Matagami mining camp: Implications for the Norita ore deposits: Economic Geology, v. 88, p. 1542–1559.

Reynolds, I.M., 1995a, Contrasted mineralogy and textural relationships in the uppermost titaniferous magnetite layers of the Bushveld Complex in the Bierkraal area north of Rustenburg: Economic Geology, v. 80, p. 1027–1048.

——1995b, The nature and origin of titaniferous magnetite-rich layers in the upper zone of the Bushveld Complex: A review and synthesis: Economic Geology, v. 80, p. 1089–1108.

Richardson, C.J., Cann, J.R., Richards, H.J., and Cowan, J.G., 1987, Metal-depleted root zones of the Troodos ore-forming hydrothermal systems, Cyprus: Earth and Planetary Science Letters, v. 84, p. 243–253.

Roberts, G.R., 1975, The geological setting of the Mattagami Lake mine, Quebec: A volcanogenic massive sulfide deposit: Economic Geology, v. 70, p. 115–129.

Romm, E.S., 1966, Flow characteristics of fractured rocks (in Russian): Moscow, Russia,Nedra, 283 p.

Rosenberg, N.D., Spera, F.J., and Haymon, R.M., 1993, The relationship between flow and permeability field in seafloor hydrothermal systems: Earth and Planetary Science Letters, v. 116, p. 135–153.

Schardt, C., Yang, J., and Large, R., 2005, Numerical heat and fluid-flow modeling of the Panorama volcanic-hosted massive sulfide district, Western Australia: Economic Geology, v. 100, p. 547–566.

Schiffman, P., and Smith, B.M., 1988, Petrology and oxygen isotope geochemistry of a fossil seawater hydrothermal system within the Solea graben, northern Troodos Ophiolite, Cyprus: Journal of Geophysical Research, v. 93, p. 4612–4624.

Schiffries, C.M., and Skinner, B.J., 1987, The Bushveld hydrothermal system: Field and petrologic evidence: American Journal of Science, v. 287, p. 566–595.

Scott, R.W., 1980, The geology and petrology of a portion of the Bell River Complex in Bourbaux Township, Quebec: Unpublished M.Sc. thesis, Toronto, Ontario, University of Toronto, 244 p.

Sharpe, J.I., 1965, Field relations of Matagami sulphide masses bearing on their disposition in time and space: Canadian Institute of Mining and Metallurgy Bulletin, v. 58, p. 951–964.

——1968, Geology and sulfide deposits of the Matagami area, Abitibi-East County: Quebec Department of Natural Resources Geological Report 137, 122 p.

Snow, D.T., 1965, A parallel plate model of fractured permeable media: Unpublished Ph.D. thesis, Berkeley, California, University of California, 331 p.

——1968, Rock fracture spacings, openings, and porosities: Journal of the Soil Mechanics and Foundations Division, Proceedings of the American Society of Civil Engineers, v. 94, p. 73–91.

——1969, Anisotropic permeability of fractured media: Water Resource Research, v. 5, p. 1273–1288.

——1970, The frequency and aperture of fractures in rocks: Journal of Rock Mechanics, v. 7, p. 23–40.

Solomon, M., Walshe, J.L., and Eastoe, C.J., 1987, Experiments on convection and their relevance to the genesis of massive sulphide deposits: Australian Journal of Earth Sciences, v. 34, p. 311–323.

Taner, M.F., Ercit, T.S., and Gault, R.A., 1998, Vanadium-bearing magnetite from the Matagami and Chibougamau mining districts, Abitibi, Quebec, Canada: Exploration and Mining Geology, v. 7, p. 299–311.

Tosdal, R.M., and Richards, J.P., 2001, Magmatic and structural controls on the development of porphyry Cu ± Mo ± Au deposits: Reviews in Economic Geology, v. 14, p. 157–181.

Trimmer, D., Bonner, B., Heard, H.C., and Duba, A., 1980, Effect of pressure and stress on water transport in intact and fractured gabbro and granite: Journal of Geophysical Research, v. 85, p. 7059–7071.

van Everdingen, D.A., 1995, Fracture characteristics of the sheeted dike complex, Troodos Ophiolite, Cyprus: Implications for permeability of oceanic crust: Journal of Geophysical Research, v. 100, p. 19957–19972.

Vilas, R.N., and Norton, D., 1977, Irreversible mass transfer between circulating hydrothermal fluids and the Mayflower stock: Economic Geology, v. 72, p. 1471–1504.

Von Herzen, R.P., and Scott, J.H., 1991, Thermal modeling for hole 735B: Proceedings of the Ocean Drilling Program, Scientific Results, v. 118, p. 349–356.

Wilcock, W.S.D., and Delaney, J.R., 1996, Mid-ocean ridge sulfide deposits: Evidence for heat extraction from magma chambers or cracking fronts?: Earth and Planetary Science Letters, v. 145, p. 49–64.

Wilson, C.R., Witherspoon, P.A., Long, J.C.S., Galbraith, R.M., Dubois, A.O., and McPherson, M.J., 1983, Large-scale hydraulic conductivity measurements in fractured granite [abs.]: International Journal of Rock Mechanics Mining Science Geomechanics Abstracts, v. 20, p. 269–276.

Witherspoon, P.A., 2000, Investigations at Berkeley on fracture flow in rocks: From the parallel plate model to chaotic systems: Geophysical Monograph 122, p. 1–58.

Witherspoon, P.A., Wang, J.S.Y., Iwai, K., and Gale, J.E., 1980, Validity of cubic law for fluid flow in deformable rock fracture: Water Resources Research, v. 16, p. 1016–1024.

Yang, K., and Scott, S.D., 1996, Possible contributions of a metal-rich magmatic fluid to a seafloor hydrothermal system: Nature, v. 383, p. 420–423.

Zhang, S., Cox, S.F., and Paterson, M.S., 2001, Microcrack growth and healing in deformed calcite aggregates: Tectonophysics, v. 355, p.17–36.

Zimmerman, R.W., and Yeo, I., 2000, Fluid flow in rock fractures: From the Navier-Stokes equation to the Cubic Law: Geophysical Monograph 122, p. 213–224.

APPENDIX

Permeability Tensor Theory

Assuming that a defined fractured rock mass volume can be considered a homogeneous anisotropic porous medium, it obeys Darcy's Law, which states that the apparent seepage velocity v_i is related to the gradient of total hydraulic head ϕ by a coefficient k_{ij}, known as the permeability tensor (Oda, 1985):

$$v_i = -\frac{g}{\nu} k_{ij} \frac{\partial \phi}{\partial x_i} = \frac{g}{\nu} k_{ij} J_i, \tag{A.1}$$

where g is the gravitational acceleration, ν is the kinematic viscosity, and $J_i = -\partial\phi/\partial x_i$. As noted by Oda (1985), it is not guaranteed that every rock mass can be simulated by an equivalent porous medium with a symmetrical permeability tensor. However, numerical studies by Long et al. (1982) and Oda (1985) have indicated that rock masses containing a significant number of discontinuities do in fact approach such behavior.

Cracks

Consider a cubic flow region of volume V homogeneously cut by $m^{(V)}$ cracks, the centers of which occur at random throughout the volume. Reliable information regarding the shape of the actual cracks is usually unattainable. Therefore, circular disc-shaped cracks of diameter $\boldsymbol{r}$ and aperture $\boldsymbol{t}$ are assumed (Oda, 1985). As a result, each crack is associated with a void volume equal to $\pi \boldsymbol{r}^2 \boldsymbol{t}/4$. The orientation of a crack is defined by two parallel but of-opposite-direction unit vectors $\boldsymbol{n}^{(+)}$ and $\boldsymbol{n}^{(-)}$ that are normal to the major plane of the crack. In the theory that follows, $\boldsymbol{n}$ will denote both $\boldsymbol{n}^{(+)}$ and $\boldsymbol{n}^{(-)}$ and is oriented over the entire solid angle Ω corresponding to the surface of a unit sphere.

Derivation of the permeability tensor:

Throughout this study it is assumed that the uncracked gabbro and/or anorthosite of the Bell River Complex are impermeable relative to the cracked rock, at least to a first-order approximation. As a result, fluid flow is restricted to the cracks, and the resultant flow velocity v_i is defined by

$$v_i = \frac{1}{V} \int_{V^{(c)}} v_i^{(c)} dV^{(c)}, \tag{A.2}$$

where superscript (c) denotes the local velocity and volume associated with the cracks. The unit vectors normal to the cracks are oriented inside a small solid angle $d\Omega$ around $\boldsymbol{n}$, and the apertures and diameters range through $t + dt$ and $r + dr$, respectively. Oda (1985) introduced a probability density function $E(\boldsymbol{n},r,t)$ to describe the directional distribution of crack surfaces in such a way that

$$\int_0^{t_{max}} \int_0^{r_{max}} \int_0^{\Omega} E(\boldsymbol{n},r,t) d\Omega dr dt = 1. \tag{A.3}$$

Recalling that the centers of cracks occur at random in the flow region, the crack geometry is completely specified by the density function plus the number of cracks (Oda, 1985).

Let dN represent a number of $(\boldsymbol{n},r,t)$ cracks with centers located inside a flow region of volume V. To estimate the actual number (dN), the probability of $(\boldsymbol{n},r,t)$ cracks is multiplied by the total number of cracks $m^{(V)}$

$$dN = m^{(V)} E(\boldsymbol{n},r,t)\, d\Omega\, dr\, dt. \tag{A.4}$$

Because each $(\boldsymbol{n},r,t)$ crack produces a void volume of $\pi r^2 t/4$, the total void volume dV associated with the $(\boldsymbol{n},r,t)$ cracks is given by

$$dV^{(c)} = \frac{\pi r^2 t}{4} dN \tag{A.5A}$$

or

$$dV^{(c)} = \frac{\pi r^2 t}{4} m^{(V)} E(\boldsymbol{n},r,t)\, d\Omega\, dr\, dt. \tag{A.5B}$$

If the overall head gradient $\mathbf{J}$ is uniformly distributed over the entire flow domain, the head gradient $\mathbf{J}^{(c)}$ along an $(\boldsymbol{n},r,t)$ crack is given by

$$J_i^{(c)} = (\delta_{ij} - n_i n_j) J_i, \tag{A.6}$$

where δ_{ij} is the Kronecker delta. As noted by Oda et al. (1987), the assumption of a uniformly distributed head gradient needs to be examined experimentally. Unfortunately, there are currently no experimental data to check the validity of equation (A.6). However, numerical experiments by Long et al. (1982) and Long and Witherspoon (1985) have suggested that the gradient of hydraulic head is nearly uniform if many fractures are present to create a sufficient number of flow paths. Fluid movement in a crack of indefinite length can be idealized by laminar flow between parallel planar plates with aperture t. The associated mean fluid velocity is given by

$$v_i^{(c)} = \frac{1}{12} \frac{g}{\nu} t^2 J_i^{(c)}. \tag{A.7}$$

However, it is likely inaccurate to assume in general that actual cracks extend indefinitely. Instead it may be more appropriate for $(\boldsymbol{n},r,t)$ cracks to define a flow velocity such as (Oda, 1985)

$$v_i^{(c)} = \lambda \frac{g}{\nu} t^2 J_i^{(c)}, \tag{A.8}$$

where λ is a dimensionless constant governed by $0 < \lambda < 1/12$. λ approaches 1/12 with the increasing length of the related cracks. Given the highly developed fracture networks at many of the sites and in interest of eliminating as many extraneous variables as possible, λ was kept constant at 1/12 throughout this study.

By combining equations (A.6) and (A.8), the apparent velocity associated with $(\boldsymbol{n},r,t)$ cracks is written as

$$v_i^{(c)} = \lambda \frac{g}{\nu} t^2 (\delta_{ij} - n_i n_j) J_i. \tag{A.9}$$

Finally, through equations (A.5B) and (A.9), equation (A.2) can be rewritten as

$$v_i = \lambda \frac{g}{V} \left[\frac{\pi \rho}{4} \int_0^{t_{max}} \int_0^{r_{max}} \int_0^{\Omega} r^2 t^3 (\delta_{ij} - n_i n_j) E(\boldsymbol{n},r,t)\, d\Omega\, dr\, dt \right] J_i, \tag{A.10}$$

where ρ is the volume density of cracks defined by $\rho = m^{(V)}/V$.

Comparison of equation (A.10) with Darcy's Law (eq A.1] yields an equivalent permeability tensor $k_{ij}^{(c)}$ for the crack system as follows (Oda, 1985):

$$k_{ij}^{(c)} = \lambda (P_{kk}\delta_{ij} - P_{ij}) , \quad (A.11)$$

where

$$P_{ij} = \frac{\pi\rho}{4}\int_0^{t_{max}}\int_0^{r_{max}}\int_0^{\Omega} r^2 t^3 n_i n_j E(\boldsymbol{n}, r, t)\, d\Omega\, dr\, dt , \quad (A.12A)$$

or

$$P_{ij} = \frac{\pi}{4V}\int_0^{t_{max}}\int_0^{r_{max}}\int_0^{\Omega} r^2 t^3 n_i n_j dN , \quad (A.12B)$$

and

$$P_{kk} = P_{11} + P_{22} + P_{33} . \quad (A.13)$$

P_{ij}, defined by Oda (1985) as the crack tensor, is a symmetric second-rank tensor relating only to the crack geometry (length, aperture, orientation). Equation (A.11) assumes that the flow region is fully divided by cracks, thus providing multiple flow paths. Furthermore, equation (A.13) produces a nonzero permeability, even when P_{ij} becomes negligibly small. However, in actuality, the flow region (especially at larger scales) may become impermeable from a loss of connectivity between cracks. Oda (1985) provides a minor modification to equation (A.11) to account for such a scenario. However, it is omitted here because of the abundant cracks at all sample locations.

Application of the permeability tensor

As discussed above, a lack of outcrop exposure in the third dimension limited a majority of the sample sites to collection of two-dimensional data and tensor calculation. However, three-dimensional data were obtained from five sites to complement two-dimensional data. The data from these five sites indicate that there are no significant discrepancies between the magnitude or orientation of the two- and three-dimensional permeability tensors calculated. Because all relevant information related to crack geometry was collected in the field, an additive form, rather than the integral form, of equation (A.12B) is used to calculate the crack tensors:

$$P_{11} = \frac{\pi}{4V}\sum_{k=1}^{m^{(V)}} Tr^{(k)} (t^{(k)})^3 \cos\theta^{(k)}\cos\theta^{(k)} , \quad (A.14A)$$

$$P_{12} = \frac{\pi}{4V}\sum_{k=1}^{m^{(V)}} Tr^{(k)} (t^{(k)})^3 \cos\theta^{(k)}\sin\theta^{(k)} , \quad (A.14B)$$

$$P_{13} = \frac{\pi}{4V}\sum_{k=1}^{m^{(V)}} Tr^{(k)} (t^{(k)})^3 \cos\theta^{(k)}\cos\theta^{(k)} , \quad (A.14C)$$

$$P_{21} = \frac{\pi}{4V}\sum_{k=1}^{m^{(V)}} Tr^{(k)} (t^{(k)})^3 \sin\theta^{(k)}\cos\theta^{(k)} , \quad (A.14D)$$

$$P_{22} = \frac{\pi}{4V}\sum_{k=1}^{m^{(V)}} Tr^{(k)} (t^{(k)})^3 \sin\theta^{(k)}\sin\theta^{(k)} , \quad (A.14E)$$

$$P_{23} = \frac{\pi}{4V}\sum_{k=1}^{m^{(V)}} Tr^{(k)} (t^{(k)})^3 \sin\theta^{(k)}\cos\theta^{(k)} , \quad (A.14F)$$

$$P_{31} = \frac{\pi}{4V}\sum_{k=1}^{m^{(V)}} Tr^{(k)} (t^{(k)})^3 \cos\theta^{(k)}\cos\theta^{(k)} , \quad (A.14G)$$

$$P_{32} = \frac{\pi}{4V}\sum_{k=1}^{m^{(V)}} Tr^{(k)} (t^{(k)})^3 \cos\theta^{(k)}\sin\theta^{(k)} , \quad (A.14H)$$

$$P_{33} = \frac{\pi}{4V}\sum_{k=1}^{m^{(V)}} Tr^{(k)} (t^{(k)})^3 \cos\theta^{(k)}\cos\theta^{(k)} , \quad (A.14I)$$

where the superscript k refers to the kth crack among $m^{(V)}$ cracks, $\theta^{(k)}$ is the angle of inclination of $\boldsymbol{n}^{(k)}$ to the reference axis x_1 (which corresponds to a bearing of 090°; note that n_i in (A.12B) is a direction cosine of $\boldsymbol{n}$ with reference to a selected axis x_i, therefore, for example, $n_1 n_2$ is given by $\cos\theta^{(k)}{}_1\cos\theta^{(k)}{}_2 = \cos\theta^{(k)}{}_1\sin\theta^{(k)}{}_1 = \cos\theta^{(k)}\sin\theta^{(k)}$), and T (= r) is the depth of cracks (Oda, 1985). However, since T does not affect two-dimensional results, it is set to unity for two-dimensional calculations (noting that V/T = the area of the flow region for two-dimensional calculations). The resulting crack tensor, equation (A.15), is reduced to its principal axis form, equation (A.16), through the Quadratic theorem (two-dimensional tensor) or Vieta's theorem (three-dimensional tensor), as outlined in Borisenko and Tarapov (1968) and Ioannou (2004), and is then converted to a permeability tensor via equations (A.11) and (A.13).

$$[P_{ij}] = \begin{bmatrix} P_{11} & P_{12} \\ P_{21} & P_{22} \end{bmatrix}, \quad \text{(A.15A; two-dimensional)}$$

$$[P_{ij}] = \begin{bmatrix} P_{11} & P_{12} & P_{13} \\ P_{21} & P_{22} & P_{23} \\ P_{31} & P_{32} & P_{33} \end{bmatrix}, \quad \text{(A.15B; three-dimensional)}$$

$$[P_{ij}] = \begin{bmatrix} P_{11} & 0 \\ 0 & P_{22} \end{bmatrix} = \begin{bmatrix} P_1 & 0 \\ 0 & P_2 \end{bmatrix}, \quad \text{(A.16A; two-dimensional)}$$

$$[P_{ij}] = \begin{bmatrix} P_{11} & 0 & 0 \\ 0 & P_{22} & 0 \\ 0 & 0 & P_{33} \end{bmatrix} = \begin{bmatrix} P_1 & 0 & 0 \\ 0 & P_2 & 0 \\ 0 & 0 & P_3 \end{bmatrix}. \quad \text{(A.16B; three-dimensional)}$$

Orientation conventions

The strike of each vein is defined by a normal vector $\boldsymbol{n}$. The orientation of each $\boldsymbol{n}$ is initially defined as an azimuth $n^{(k)}{}_{azimuth}$, where $180° < n^{(k)}{}_{azimuth} < 0°$.

Following the methodology of Oda (1985), all $\boldsymbol{n}$ strike orientations are referenced with respect to the x_1 axis ($n^{(k)}x_{1azimuth}$), which corresponds to an azimuth of 090° (Fig. A.1). Furthermore, using a right-hand rule convention, angles measured counterclockwise from the x_1 axis (in the x_1-x_2 horizontal plane) are positive, whereas angles measured clockwise are negative. Therefore, $n^{(k)}x_{1azimuth} = 90° - n^{(k)}{}_{azimuth}$, which is the value subsequently used to calculate the permeability tensors.

Following the methodology of Oda (1985), the dips of the vein normals ($\boldsymbol{n}$) (three-dimensional calculation) are referenced with respect to the x_3 axis (zenith; Fig. A.2). Because the dip of $\boldsymbol{n}$ is measured with respect to x_3, whereas the dip of

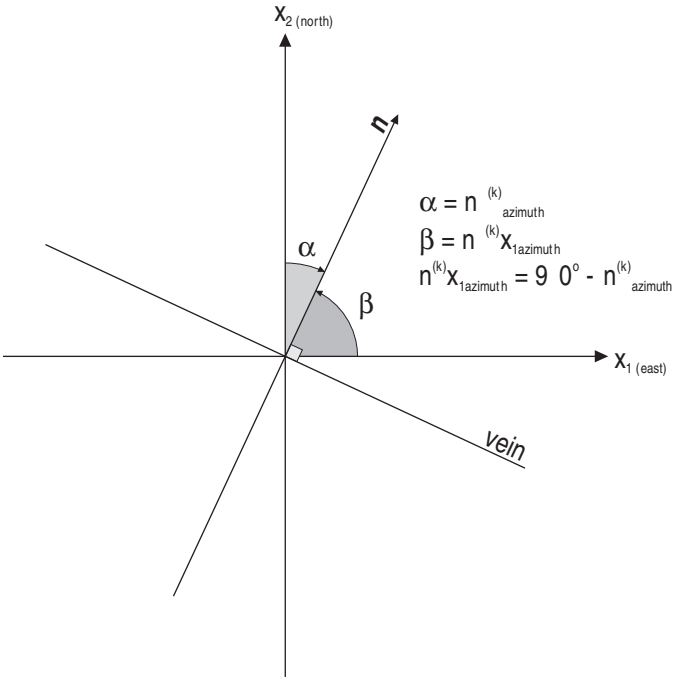

FIG. A1

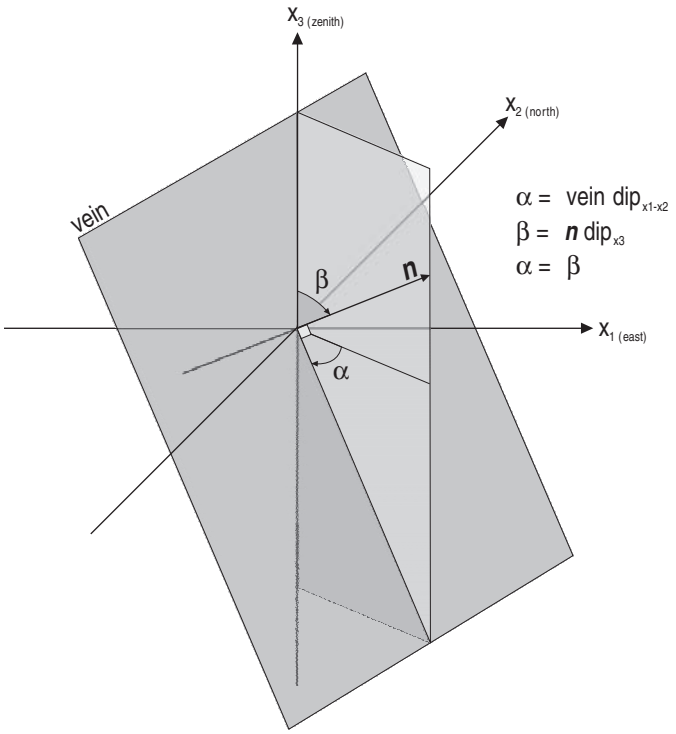

FIG. A2

the vein is measured with respect to the horizontal plane (defined by the x_1-x_2 axes), the dip of ***n*** is numerically equivalent to the dip of the vein. Applying a right-hand rule convention, dip angles of ***n*** measured counterclockwise from the x_3 axis (in the x_1-x_3 plane) are positive (i.e., easterly vein dip), whereas angles measured clockwise are negative (i.e., westerly vein dip).

The reduction of the crack tensor to principal axes introduces a new set of axes x_1', x_2', and x_3', which are not coincident with the original x_1, x_2, and x_3 axis system defined above, and the orientation of the new axes x_r' differs for each distinct sample. Therefore, to standardize the orientation of all tensors, the trend (with respect to north) and plunge (with respect to the horizontal) of each tensor is back-calculated from the orientation of the reduced principal axes x_r'. Details of this back-calculation are presented in Borisenko and Tarapov (1968) and Ioannou (2004).